



INSTITUTO
UNIVERSITÁRIO
DE LISBOA

Molecular Communication Schemes for Extreme Environments in Future Wireless Networks

Duarte Miguel Leite Casaleiro

Master Degree in Telecommunications and Computer Engineering

Supervisor:

PhD Nuno Manuel Branco Souto, Associate Professor (with Habilitation),

Iscte - Instituto Universitário de Lisboa

Co-Supervisor:

PhD João Carlos Marques Silva, Assistant Professor,

Iscte - Instituto Universitário de Lisboa

September, 2024



TECHNOLOGY
AND ARCHITECTURE

Department of Information Science and Technology

**Molecular Communication Schemes for Extreme
Environments in Future Wireless Networks**

Duarte Miguel Leite Casaleiro

Master Degree in Telecommunications and Computer
Engineering

Supervisor:

PhD Nuno Manuel Branco Souto, Associate Professor (with
Habilitation),

Iscte - Instituto Universitário de Lisboa

Co-Supervisor:

PhD João Carlos Marques Silva, Assistant Professor,

Iscte - Instituto Universitário de Lisboa

September, 2024

Acknowledgments

I would like to begin by expressing my sincerest gratitude to my supervisor PhD Nuno Souto and to my co-supervisor PhD João Silva for their guidance and support throughout this dissertation. A special thanks to my supervisor PhD Nuno Souto for his unwavering support and dedication, which motivated me throughout this journey. It was truly an honor to work and learn from such an outstanding professor.

Furthermore, I would like to acknowledge Instituto de Telecomunicações (IT) for supporting me with the necessary resources for this work. In addition, I would like to express my gratitude to Iscte - Instituto Universitário de Lisboa for promoting a culture of mutual support and for providing a world of opportunities to its students. After five years, which were both long and brief, I truly believe that there is no better place to learn. I would like to extend my gratitude to the exceptional teachers with whom I had the privilege of learning from. In particular, I would like to thank PhD Rui Marinheiro for trusting me with the opportunity to work as a laboratory monitor. It was a privilege to learn from you during this academic journey.

To my dear friends Rodrigo and Olek, thank you for supporting me and making these last five years the most memorable of my life. To my beloved colleagues and friends Filipe, Henrique, Gonçalo, Margarida, Miguel, Pedro and Roberto, It was such a pleasure to be at your side during this journey. Finally, to my lifelong friends Afonso and Tomás, thank you for always being by my side and encouraging me throughout this whole process.

I would like to express my sincerest gratitude to my girlfriend, Ana, for her unwavering patience, encouragement, support and love. Thank you for being part of my life, for your unconditional encouragement for me to follow my dreams and for your belief in me, even when I am unable to believe in myself.

I would also like to thank my family for their unconditional support. In particular, I would like to acknowledge the indispensable role of my parents in always supporting and believing in me and providing me with the necessary resources to pursue my dreams. To my brother Nuno and to my cousins Marta and André, thank you for being a role model and for always inspiring and advising me. Thank you to my aunts Branca, Teresa and Zélia, to my grandmother and to my cousins, specially to the loving little ones, António and Flor. Your support was truly essencial throughout my academic career. Finally, I want to acknowledge those who sadly are no longer in this world. Your presence in my life was invaluable and I will forever remind and cherish the memories we shared.

Resumo

O conceito de “Internet das Bio-Nano Coisas” surgiu devido às suas possibilidades revolucionárias que transcendem os sistemas tradicionais de comunicação sem fios. A Comunicação Molecular surge como uma potencial peça central para este paradigma, permitindo aplicações em ambientes desafiantes.

No entanto, este tipo de comunicação, que se baseia frequentemente na difusão molecular, sofre de uma elevada interferência inter-simbólica (IIS), que deteriora a transmissão da informação. Para lidar com a forte IIS, bem como com o curto tempo de coerência típico do canal molecular, este trabalho considera a adoção de uma abordagem baseada em dados para realizar uma detecção não coerente no recetor. Em particular, investigamos o desempenho de uma Rede Neural Convolutiva (CNN) unidimensional de baixa complexidade baseada em camadas convolucionais causais dilatadas, uma Rede Neural Recorrente baseada em Unidades Recorrentes Gated Recurrent (GRU-RNN) e uma Rede Neural Convolutiva unidimensional combinada com uma Rede Neural Recorrente de Unidades Recorrentes Gated Recurrent (CNN-RNN 1-D), para as tarefas de detecção e sincronização de símbolos.

Inicialmente, estudamos o desempenho dos detetores baseados em Redes Neurais (RNs) propostos assumindo sincronização prévia entre o transmissor e o recetor e, posteriormente, estendemos a abordagem para cenários sem sincronização prévia. Além disso, investigamos também a robustez das RNs propostas face a variações desconhecidas na distância entre o emissor e o recetor, bem como no coeficiente de difusão. Finalmente, os resultados apresentados neste trabalho levam à conclusão de que a implementação de RNs para sincronização e detecção não-coerente pode ser uma abordagem muito eficaz para o desafiante canal molecular.

PALAVRAS CHAVE: 6G, futuras redes sem fios, comunicação molecular, redes neuronais

Abstract

The concept of Internet of Bio-Nano Things (IoBNT) has emerged due to its revolutionary possibilities that transcend traditional wireless communication systems. Molecular Communication (MC) arises as a potential centrepiece for this paradigm, enabling applications in challenging environments.

However, this type of communication, which often relies on molecular diffusion, suffers from a high inter-symbol interference (ISI), which deteriorates the reliability of the transmission. To cope with the strong ISI as well as the typical short coherence time of the MC channel, this work considers the adoption of a data-driven approach to accomplish non-coherent based detection at the receiver. In particular, we investigate the performance of a low complexity one-dimensional Convolutional Neural Network (CNN) based on dilated causal convolutional layers, a Gated Recurrent Unit based Recurrent Neural Network (GRU-RNN) and a one-dimensional Convolutional Neural Network combined with a Gated Recurrent Unit Recurrent Neural Network (1-D CNN-RNN) aimed at the tasks of symbol detection and synchronization.

Initially, we study the performance of the proposed Neural Network (NN) based detectors assuming prior synchronisation between the transmitter and the receiver and, afterwards, we extend the approach for scenarios without prior synchronisation. Furthermore, we also investigate the robustness of the proposed NNs schemes against unknown variations in the distance between the transmitter and the receiver as well as in the diffusion coefficient. Finally, the results presented in this work lead to the conclusion that the implementation of NNs for both synchronisation and non-coherent detection can be a very effective approach for the challenging MC channel.

KEYWORDS: 6G, future wireless networks, molecular communication, neural networks.

Contents

Acknowledgments	i
Resumo	iii
Abstract	v
List of Figures	ix
List of Tables	xi
List of Acronyms	xiii
Chapter 1. Introduction	1
1.1. Background and Motivation	1
1.2. Research questions and objectives	2
1.3. Methodology	3
1.4. Structure	3
Chapter 2. State of the art	5
2.1. The Internet of Bio-nano Things Paradigm	5
2.2. Fundamentals of Molecular Communication	6
2.3. Bio-cyber Interface	7
2.4. Molecular Channel via Diffusion	7
2.5. Noise	8
2.6. Transmitter	8
2.7. Receiver	10
2.8. Modulation Techniques for MC	11
2.8.1. Concentration Shift Keying - CSK	11
2.8.2. Molecular Shift Keying - MoSK	12
2.8.3. Pulse Position Modulation - PPM	12
2.9. Neural Networks	13
2.9.1. Supervised and Unsupervised Learning	14
2.9.2. Convolutional Neural Networks - CNNs	14
2.9.3. Recurrent Neural Networks - RNNs	15
2.9.4. Long Short-term Memory (LSTM) Layers	15
2.9.5. Gated Recurrent Units (GRU) Layers	16
2.9.6. Machine Learning applied to MC	17
	vii

Chapter 3. DNN-based MC detectors	19
3.1. Transmitted Signal	19
3.2. Signal Pulse Type	20
3.3. Channel Model	21
3.4. Signal Detection	22
3.4.1. Direct Non-coherent Detection	22
3.4.2. Neural Network Based Detection	23
3.4.3. Recurrent Neural Networks (RNNs)	27
3.4.4. 1-D Convolutional Neural Network based on dilated causal convolutional layers (1-D CNN)	29
3.4.5. 1-D Convolutional Neural Network combined with a Gated Recurrent Unit based Recurrent Neural Network (1-D CNN-RNN)	31
3.5. Frame Synchronisation	32
Chapter 4. Numerical Results	35
4.1. Simulation Parameters	35
4.2. Neural Network based detection with perfect synchronisation	36
4.2.1. Distance variations	37
4.2.2. Diffusion variations	38
4.2.3. Neural Network based detection with perfect synchronisation facing variations in the molecular channel	39
4.3. Neural Networks for the synchronisation and detection process	41
4.3.1. Neural Networks for the synchronisation and detection process facing variations in the distance and in the diffusion coefficient	45
Chapter 5. Conclusions and Future Work	47
5.1. Future Work	48
References	49
Appendix A. Research Article	53

List of Figures

Figure 2.1	Example of a IoBNT network architecture, adapted from [3] and [10].	5
Figure 2.2	Physical principles of MC, adapted from [1].	6
Figure 2.3	Transmitter models: (1) Point Transmitter; (2) Volume Transmitter; (3) Ion-Channel Based Transmitter, from [13].	9
Figure 2.4	Receiver models: (1) Passive Receiver; (2) Fully-absorbing Receiver; (3) Reactive Receiver, from [13].	10
Figure 2.5	Concentration Shift Keying, adapted from [4].	11
Figure 2.6	Molecular Shift Keying, adapted from [4].	12
Figure 2.7	Pulse Position Modulation, adapted from [9].	12
Figure 2.8	Representation of the connections to a neuron, adapted from [14].	13
Figure 2.9	Example of a CNN architecture, from [14].	15
Figure 2.10	Example of a RNN architecture, from [23].	15
Figure 2.11	Structure of a LSTM unit.	16
Figure 2.12	Structure of a GRU unit.	17
Figure 3.1	OOK modulation scheme, adapted from [4].	19
Figure 3.2	Frame structure.	20
Figure 3.3	Unipolar NRZ pulse.	20
Figure 3.4	Demodulation process for the direct non-coherent detection. . . .	22
Figure 3.5	Demodulation process for the NN-based non-coherent detection. . .	22
Figure 3.6	BER comparison between the regression and the classification network.	26
Figure 3.7	BER comparison between the single-layer LSTM-RNN and GRU-RNN.	28
Figure 3.8	BER comparison between the single-layer GRU-RNN and the low-complexity GRU-RNN.	29
Figure 3.9	Architecture of a 1-D CNN based on dilated causal convolutional layers, adapted from [33].	30
Figure 3.10	Block diagram for each of the proposed NN architectures.	32
Figure 3.11	Demodulation process for method 1.	33
Figure 3.12	Demodulation process for method 2.	34
Figure 3.13	Demodulation process for method 3.	34

Figure 4.1	BER comparison between the NNs and the direct non-coherent detection.	37
Figure 4.2	BER comparison between the NNs and the direct non-coherent detection for each considered distance value.	38
Figure 4.3	BER comparison between the NNs and the direct non-coherent detection for each considered diffusion coefficient error.	39
Figure 4.4	BER comparison between the NNs and the direct non-coherent detection, considering variations in the distance and in the diffusion coefficient.	40
Figure 4.5	Direct non-coherent detection for the considered Barker Codes. . .	42
Figure 4.6	NNs applied to each synchronisation and detection method. . . .	44
Figure 4.7	NNs applied to each synchronisation and detection method, considering variations in the distance and in the diffusion coefficient. .	46

List of Tables

Table 1.1	Differences between MC and EM communication, adapted from [7]. .	2
Table 3.1	Regression neural network architecture.	25
Table 3.2	Classification neural network architecture.	25
Table 3.3	Single-layer LSTM-RNN architecture.	27
Table 3.4	Single-layer GRU-RNN architecture.	27
Table 3.5	Low-complexity GRU-RNN architecture.	28
Table 3.6	1-D CNN based on dilated causal convolutional layers architecture. .	30
Table 3.7	1-D CNN-RNN architecture.	31
Table 4.1	Main parameters considered for the Monte Carlo simulations.	35

List of Acronyms

1-D	One-dimensional
6G	Sixth generation wireless systems
Adam	Adaptive Moment Estimation
ASK	Amplitude Shift Keying
BCSK	Binary Concentration Shift Keying
BER	Bit Error Rate
CNN	One-dimensional convolutional neural network based on dilated causal convolutional layers
CNNs	Convolutional Neural Networks
CNN-RNN	One-dimensional convolutional neural network combined with a gated recurrent unit based recurrent neural network
CSK	Concentration Shift Keying
CSI	Channel State Information
DNNs	Deep Neural Networks
EM	Electromagnetic Communication
GRU	Gated Recurrent Unit
GRU-RNN	Gated recurrent unit based recurrent neural network
IoBNT	Internet of Bio-nano Things
IoNT	Internet of Nano Things
IoT	Internet of Things
ISI	Inter-symbol interference
LLR	Log-likelihood ratio
LSTM	Long short-term memory
LSTM-RNN	Long short-term memory based recurrent neural network
MC	Molecular Communication
MCvD	Molecular Communication via Diffusion
MIMO	Multiple-input Multiple-output
MoSK	Molecular Shift Keying
NNs	Neural Networks
NRZ	Non-return-to-zero
OOK	On-Off Keying

PPM	Pulse Position Modulation
ReLU	Rectified linear unit
RNNs	Recurrent Neural Networks
SGD	Stochastic Gradient Descent

Introduction

1.1. Background and Motivation

Throughout history, there has been a constant pursuit for new ways to communicate in order to improve our knowledge, our society and our industries. Currently, the on-demand research work regarding to the Sixth generation wireless systems (6G), is expected to enable communications in environments that were previously considered unfeasible.

In order to fulfil these challenges, the concept of Internet of Bio-nano Things (IoBNT) has emerged due to its revolutionary possibilities that transcend the traditional wireless communication systems. IoBNT enables the formation of networks between bio-devices establishing connectivity between them, enabling a wide range of applications in various fields such as [1], [2]:

- **Health-care**
 - Health monitoring;
 - Targeted drug delivery;
 - Disease diagnosis;
 - Regenerative medicine;
- **Industry**
 - Quality control;
 - Pipeline communication for leak detection;
- **Defence**
 - Underwater communication for search-and-rescue missions;
 - Swarm control for rescue missions;

Since the goal of IoBNT is to enable communications in extreme environments, it is imperative that the devices have the ability to communicate without deteriorate the surrounding environment, thus being so-called biocompatible.

That being said, Electromagnetic Communication (EM) which has been widely studied in the area of Internet of Nano Things (IoNT), cannot be a solution as it generates radiation that can affect the intended critical environments [3]. In addition, EM at nanoscale requires wavelengths proportional to the size of the antennas [4]–[6], hence must operate in the THz range. Since the shorter the wavelength, the higher the frequency, this

implies greater attenuation for this type of communication, making it unfeasible for the applications envisaged in IoBNT [1].

Molecular Communication (MC), on the other hand, has the potential to be at the heart of this new paradigm in terms of its ability to mimic the communication between biological cells, using molecules as information carriers [2], [3], [5], [7]–[9]. MC systems are very energy-efficient as they do not require extra energy due to the Brownian motion of the molecules carrying information [7]. Another advantage of these systems is that they have an unlimited spectrum, since we can occupy the totality of the bandwidth due to the lack of limitations and regulations [5]. Furthermore, MC can also be bio-compatible with *in-vivo* applications as it does not harm the envisioned environments by emitting any kind of radiation. In table 1.1, presented below, it is possible to observe the differences between the two types of communication technologies mentioned above in a summarized form.

Communication	Energy efficient	Spectrum	Speed	Range	Biocompatible
EM	No	[0.3, 10] THz	Very High	Very Low	No
MC	Yes	None	Very Low	Very Low	Yes

Table 1.1. Differences between MC and EM communication, adapted from [7].

1.2. Research questions and objectives

Despite the advantages of MC, this type of communication is still in its infancy. One of the main challenges for this type of communication is the existence of a high Inter-symbol interference (ISI) due to the slow absorption of the information molecules by the receiver [4], [8], which significantly restricts the transmission rates for this type of communication. Moreover, given the nature and the challenging environments in which MC is envisioned to be deployed, the modulation, coding and detection schemes must be of reduced complexity to ensure a more robust communication.

Consequently, there are still unsolved problems related to the detection of the signal propagating through the molecular channel and efficient modulation schemes to correctly identify the information embedded in the molecular patterns [8].

With the development of new and more complex communication methods and techniques in the Telecommunications domain, there has been an increasing adoption of deep neural networks in order to estimate the information received in the receptors. Since the molecular channel is very unpredictable due to the random Brownian motion of the molecules, this work proposes the implementation of deep Neural Networks (NNs) to be deployed in the molecular receiver, in order to detect the information that has been sent without estimating the channel itself, thus performing non-coherent detection.

With this in mind, the following research questions have been identified:

- Is it possible to implement low-complexity NN-based detectors to perform non-coherent detection of the MC signal assuming perfect synchronisation between the transmitter and the receiver?
- Is it possible to extend the design of the proposed NN-based detectors for scenarios where there is no previous synchronisation between the transmitter and the receiver?
- Is it possible to train the proposed NN-based detectors in order to enhance their robustness against unknown variations in the channel conditions?

1.3. Methodology

For the purpose of this dissertation, initially a bibliographical research was carried out using the following keywords: Molecular Communication, Neural Networks, Deep Learning, Convolutional Neural Networks and Recurrent Neural Networks.

In order to demonstrate the effectiveness of NNs in MC receivers, in this work we rely on extensive Monte Carlo simulations to evaluate the Bit Error Rate (BER) of the molecular transmission. Initially, we evaluate the performance of the proposed NN architectures for non-coherent detection assuming perfect synchronisation between the transmitter and the receiver. Afterwards, we extend the design of the proposed NNs for scenarios where there is no previous synchronisation between the transmitter and the receiver, aiming at the tasks of synchronisation and symbol detection. Finally, bearing in mind the unpredictability of the molecular channel, we evaluate the performance of the proposed NN architectures against unknown variations in the distance between the transmitter and the receiver as well as in the diffusion coefficient. At last, it is also worth noting that the data used for the training of the proposed NNs was also generated through Monte Carlo simulations.

1.4. Structure

In terms of its structure, this work is organised as follows:

- **Chapter I** presents a brief introduction to the subject matter of this dissertation, as well as the motivations and research questions that were considered;
- **Chapter II** introduces the state of the art of the concepts that will be covered throughout this dissertation;
- **Chapter III** describes the considered system model and the proposed NN architectures adopted in this work. In addition, this chapter also presents a detailed description of the proposed synchronisation methods;

- **Chapter IV** describes the numerical simulations carried out for evaluating the performance of the different NN-based detectors and presents the results of the respective simulations;
- **Chapter V** presents the conclusions of this dissertation as well as a description of potential future work to improve the proposed NN architectures.

CHAPTER 2

State of the art

In this chapter it will be presented a summarization of the concepts in the field of molecular communications.

2.1. The Internet of Bio-nano Things Paradigm

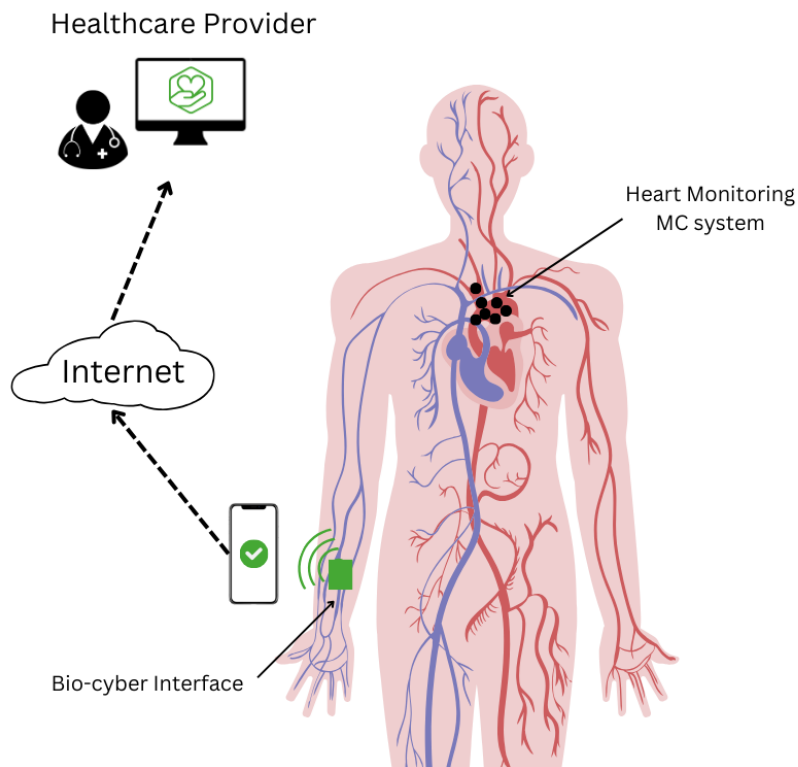


Figure 2.1. Example of a IoBNT network architecture, adapted from [3] and [10].

The relentless investigation in the field of Internet of Things (IoT) and IoNT, aggravated by its estimated billion dollar market size [11], made possible the emergence of a new paradigm called IoBNT. This concept aims to mimic biological communication used by cells in nature by making the most of biological cells, in order to enable communication between bio-compatible nanodevices, mentioned in [3] as bio-nano things. These devices operate in biological environments such as intra-body communication, that have been

considered as unfeasible with the traditional EM communication systems [1], [7]. Figure 2.1 describes an example of a IoBNT implementation.

In parallel with IoBNT, the concept of MC arises as the basis of this new paradigm. As already mentioned in chapter 1, MC has several advantages over conventional EM communication systems, as can be seen in table 1.1. One of the main advantages of MC is the fact that it has the potential to be biocompatible, enabling in-body sensing and actuation while also allowing the creation of nanonetworks of bio-nanodevices.

Furthermore, while MC enables intra-body communication, the concept for a new nanodevice called a bio-cyber interface arises as a key component for translating chemical signals into electrical signals that can be sent to the external world. [3], [7].

2.2. Fundamentals of Molecular Communication

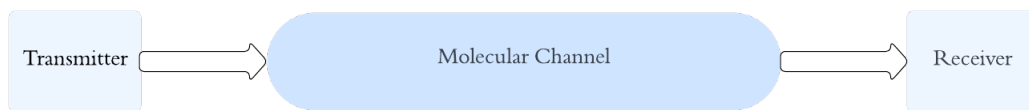


Figure 2.2. Physical principles of MC, adapted from [1].

As it can be seen in figure 2.2, MC systems can be characterized by various physical principles regarding their transmission, propagation and detection. This is equivalent to traditional communication systems, where the transmitter encodes the information in the physical properties or in characteristics of the molecules [2], [3], [5], [7]–[9]. These molecules travel through a molecular channel until they reach the receiver where, based on their concentration or quantity, they are converted into a digital signal [5].

Relatively to the transmission of information through the molecular channel, it can be passive or propulsive, as defined in [1]. Passive transmitters release the information molecules via diffusion into the molecular channel, thus not requiring any type of energy associated. This is possible due to the molecules Brownian motion, limiting the range and the transmission rate of the communication, causing a high jitter and loss rate [2]. This method can be found in cellular systems, which makes it simpler and easier to implement. Relatively to propulsive transmission, this type of transmitters induce the propagation of molecules into the communication channel [1]. With this in mind, these systems are much more complex than passive transmitters but allow higher transmission rates.

As for the propagation in the molecular channel, this can be via diffusion, active mass transport or chemical reactions [1]. Regarding to the transmission via diffusion, in this type of communication, the movement of the molecules is characterized by the random Brownian motion [5], [7], [9]. Relatively to the active mass transport transmission, it can be characterized as turbulent or laminar flow [1], where external forces induce the movement of the molecules that carry the information through the molecular channel. At last, chemical reactions are another propagation method that can be utilized in MC,

however, this mechanism has not yet been studied as much as the other alternatives mentioned before.

Regarding molecular receivers, they can be divided in two categories: passive and absorbing [9]. Passive receivers are placed at the end of the molecular channel and detect the information molecules that pass through in an indirect form [9]. On the other hand, absorbing receivers require the receiver to be placed in an invasive way. That being said, this mechanism absorbs the molecules [9] and removes them from the molecular channel [12] in order to identify the information that was sent.

2.3. Bio-cyber Interface

Bio-cyber interfaces, introduced in [3], are characterized for being bio-compatible devices capable of detecting chemical signals and translate them into electrical signals [3], [7]. The goal for these components is to accurately sense information at the molecular level, embedded in the properties of molecules, and to enable the transfer of this information to external devices outside the molecular environment.[7].

2.4. Molecular Channel via Diffusion

In the traditional communication methods, the communication channel can easily be estimated, depending on the complexity of the system. However, in MC, this is not the case given that the molecular channel is constantly changing due to the random motion of the molecules. This causes an omnidirectional propagation, which implies that the transmission rate directly depends on the communication distance [8]. That being said, the diffusion process can be very efficient for short range communication but has an increasing attenuation and very low transmission rates for long range communications [7]. Therefore, a symbol at a given time slot suffers interference from a previous symbol, causing a severe ISI [5], [8]. This effect occurs due to the slow absorption of the molecules by the receptor, causing them to remain in the communication medium for a random period of time [8]. This phenomenon leads to the conclusion that the channel in Molecular Communication via Diffusion (MCvD) has a memory [4], [8], [9].

The propagation of information in MCvD is vastly different from the means of propagation in traditional communication systems that are currently used. The Brownian motion of the molecules can be simulated by Monte Carlo simulations and is described by the following equation [7]:

$$(x_{i+1}, y_{i+1}, z_{i+1}) = ([x_i + \mathcal{N}(0, 2D\Delta t)], [y_i + \mathcal{N}(0, 2D\Delta t)], [z_i + \mathcal{N}(0, 2D\Delta t)]) . \quad (2.1)$$

Thus, the position of the information molecule after a given time interval (Δt) is given by the previous position of the molecule, adding a spatial step, following a standard Gaussian distribution ($\mathcal{N}(0, 2D\Delta t)$) with mean 0 and variance $2D\Delta t$, being D the diffusion coefficient. [9], [7], [4].

As presented in equation 2.1, the movement of the molecules is influenced by the diffusion coefficient. However, this parameter is directly affected by the temperature (T) and viscosity (μ) of the channel and by the radius of the information molecules (R). The equation presented below describes the mathematical model for the diffusion coefficient, which is given by the Stokes-Einstein relation [9], [4] as

$$D = \frac{k_B T}{\delta \pi \mu R} \quad [m^2/s] , \quad (2.2)$$

where k_B is the Boltzmann constant ($k_B = 1.38 \times 10^{-23} J/K$) and δ is the boundary of the molecular channel. Additionally, it is important to mention that δ is determined by the relation between the information molecules and the molecules in the fluid [9]. If the information molecules are bigger than the fluid particles, this parameter is equal to 6, if not, δ has a value of 4. For the investigation proposed in this work, we consider a scenario where $\delta = 6$.

2.5. Noise

Throughout the communication process, there are several physical effects that introduce noise, leading to a deterioration in the communication itself. Despite its differences with other traditional communication systems, MC also suffers from the introduction of noise such as: emission noise, diffusion noise, reception noise and environment noise [4], [8].

Diffusion noise occurs due to the random motion of the information molecules, already described and mentioned in section 2.4. On the other hand, emission and reception noise take place when the information passes through the transmitter or the receiver. Finally, environment noise arises due to the chemical reactions that happen when the information molecules travel through the molecular channel or due to their degradation over time [4].

2.6. Transmitter

As already mentioned in section 2.2, the transmitter encodes the information in the physical properties of the molecules to be sent through the molecular channel passively (via diffusion) or actively (by propulsive transmission). For this to be possible, this device is composed by three units. Firstly, a central processing unit [4] encodes the information into the physical properties of the molecules, choosing an adequate modulation scheme. Then, a release unit [4] controls the release of the information molecules into the molecular channel, according to the instructions of the central processing unit. Finally, a power unit [4], [10] is required to provide energy to the components of the device.

In order to guarantee the functionality of this type of devices, in [10] there were identified four main requirements:

- Miniaturization - The size constraints add several concerns relatively to the power storage. However, energy harvesting techniques may be implemented to overcome this difficulty;

- Molecule Reservoir - At nanoscale, the size of the reservoir is very limited, preventing the accumulation of a large number of molecules. This problem can be avoided by recurring to synthesized bacteria in order to produce the information molecules to be used;
- Biocompatibility - Given that molecular communication is envisioned for bio-environments such as the human body, this type of devices cannot contain any kind of toxic component;
- Performance - For the applications proposed for MC, it is essential to ensure that there is no leakage of molecules into the molecular channel.

Furthermore, in [13], there were identified three transmitter models regarding their geometry and generation/release mechanisms as it can be observed in figure 2.3:

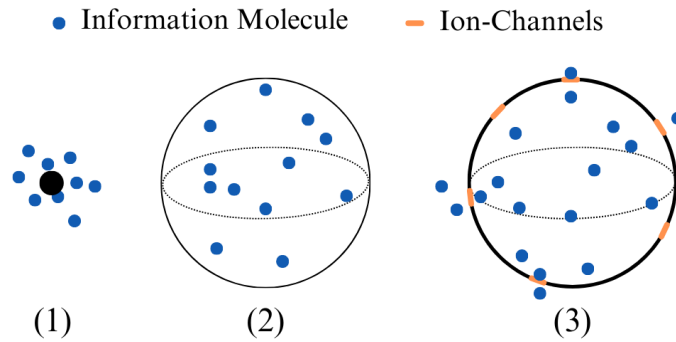


Figure 2.3. Transmitter models: (1) Point Transmitter; (2) Volume Transmitter; (3) Ion-Channel Based Transmitter, from [13].

- (1) The **Point Transmitter** is the simplest model since it considers the transmitter as a one-dimensional point. That being said, the geometry of the device does not affect the transmission process. Additionally, it is assumed that N_{molec} molecules are generated instantaneously, not taking into account the effects of the release and generation of molecules into the molecular channel;
- (2) Unlike the Point Transmitter, in the **Volume Transmitter** model, the geometry of the transmitter is taken into account and it is assumed that N_{molec} molecules are distributed throughout the volume of the reservoir. Nevertheless, this model does not consider effects in the release/generation process of the information molecules;
- (3) The **Ion-Channel Based Transmitter** is the most realistic of the models, with not only the geometry but also the release and generation mechanisms being taken into account. This model assumes ion-channels in the reservoirs membrane that, when are open, allow the transmission of the N_{molec} molecules via diffusion.

2.7. Receiver

Molecular receivers are capable of detecting the arrival of molecules and translating their physical properties into information. With this in mind, this kind of devices are composed by three distinct units. Firstly, a detection unit [4], [10] senses the targeted particles that arrive through the molecular channel. Then, based on the output of the detection unit, a processable signal is generated by a transducer unit [10]. Finally, a processing unit [4], [10] decodes the information that was sent by the transmitter.

In [10], four main requirements for the design of molecular receivers were identified:

- In Situ Operation - Given the high error rates for this type of communication, it is not convenient to rely in the decoding of the received information by external devices. With this in mind, the processing of the information must be done in the receptor itself;
- Continuous Operation - The receiver must always be monitoring the molecular channel in order to detect the information molecules;
- Miniaturization - Similarly to the transmitters described in the section 2.6, the size constraints impose several problems, one of them relatively to the power storage;
- Biocompatibility - The device should not have any kind of toxic component in its composition so it does not harm the surrounding environment;

Since experimental studies are difficult to implement and this field of investigation is still in its infancy, some studies rely exclusively on simulations. Therefore, in [10], the following receiver models were identified as it can be observed in figure 2.4:

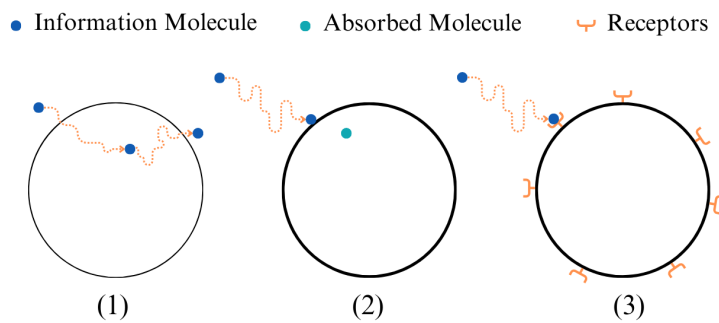


Figure 2.4. Receiver models: (1) Passive Receiver; (2) Fully-absorbing Receiver; (3) Reactive Receiver, from [13].

- (1) The model of a **Passive Receiver** assumes a receiver where N_{rx} molecules can pass through the receiver's membrane without disturbing their own movement;
- (2) In a **Fully-absorbing Receiver**, it is assumed that N_{rx} molecules are absorbed by the receiver's membrane, taking the geometry of the receiver into account;

- (3) The **Reactive Receiver** model is the most realistic, relying on protein structures located on the receiver’s membrane, called receptors. These structures are capable of binding to specific molecules, thereby resembling antennas in traditional communication systems.

2.8. Modulation Techniques for MC

The Modulation process consists of encoding the information to be transmitted into the physical properties of the molecules. In [9] are defined several modulation techniques for MC:

- A **concentration-based** approach relies in the representation of information by the number of molecules that were released into the molecular channel;
- For **type-based** modulations, the information can be encoded in the type of information molecules;
- **Timing-based** techniques can be used to represent information based on the time of the release of the information molecules;
- Similarly to conventional communication systems, **spatial** techniques can be used in MC to encode information in the spatial position of the transmitter, making it more suitable for multi-antenna systems;
- Finally, there are also **hybrid** techniques, which consists in the combination of two or more modulation schemes.

2.8.1. Concentration Shift Keying - CSK

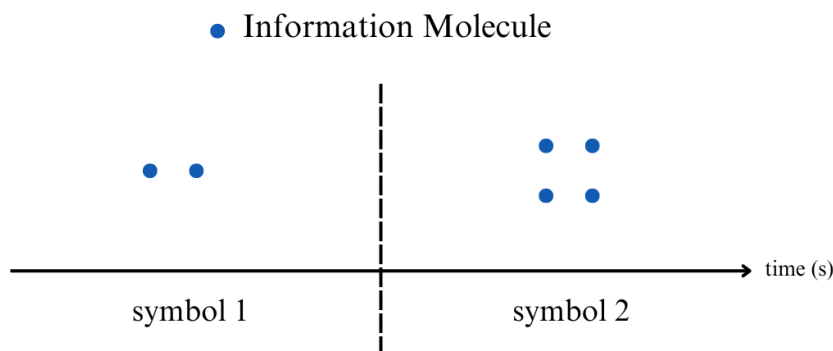


Figure 2.5. Concentration Shift Keying, adapted from [4].

Concentration Shift Keying (CSK) is a concentration-based modulation scheme for MC where the information is encoded in the concentration of the information molecules [4]. For this technique, each time slot corresponds to a single symbol [9]. Furthermore, CSK has very low complexity and resembles Amplitude Shift Keying (ASK) in traditional

communication systems. However, this modulation scheme is more affected by the noise in the molecular channel [9].

2.8.2. Molecular Shift Keying - MoSK

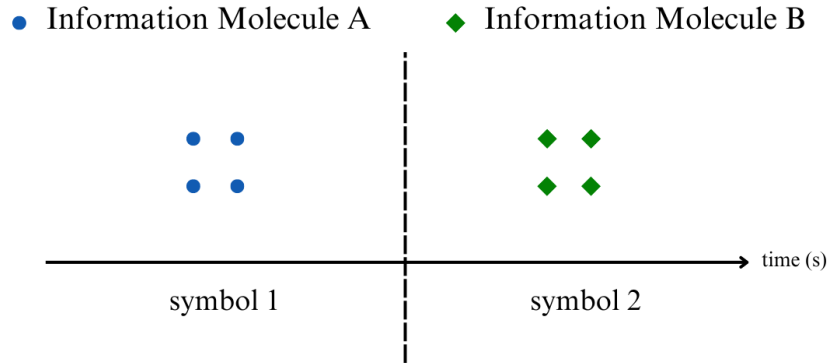


Figure 2.6. Molecular Shift Keying, adapted from [4].

Molecular Shift Keying (MoSK) is described as a type-based modulation technique [4], [9] where different types of molecules are sent into the molecular channel. Therefore, it is required to have a receptor capable of detecting multiple information molecules. The main advantage of this modulation scheme is that, once they are different from each other, the information molecules are orthogonal [9]. Although this is beneficial for reducing ISI, this type of technique is more complex in comparison to CSK.

2.8.3. Pulse Position Modulation - PPM

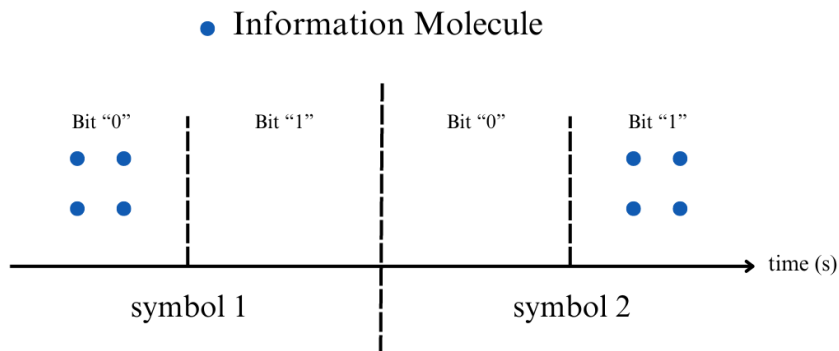


Figure 2.7. Pulse Position Modulation, adapted from [9].

The Pulse Position Modulation (PPM) is a time-based modulation scheme that encodes the information in the time of the release of the information molecules [9]. Therefore, the bit interval is divided in two halves, each one corresponding to the slot of transmission for each bit [4].

2.9. Neural Networks

Neural Networks are inspired in human neurons, since their operation mimics the processes that occur in the human nervous system. With this in mind, each connection is formed by a neuron that receives the input and performs a non-linear function to the sum of the values in the input [14], in order to return an output. Figure 2.8 presents the structure of a simple neural network connection for a better understanding of this architecture. In this case, x_i and y_i correspond to the input and output, respectively. Furthermore, the weights, represented by w_i , define the relevance of the respective input to the output returned by the neuron. Finally, $f()$ in the non-linear function applied inside the neuron and b is denominated as the bias.

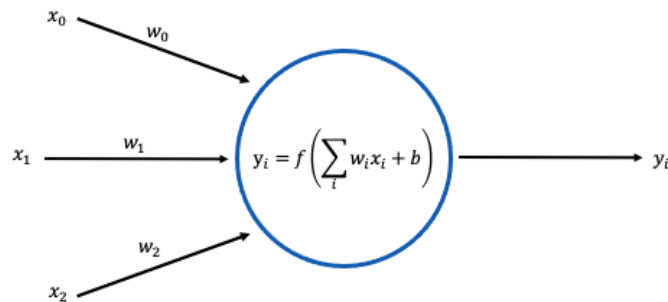


Figure 2.8. Representation of the connections to a neuron, adapted from [14].

A NN is formed by an input and output layer, and can also present a hidden layer in the middle. Therefore, the values inserted in the input layer are propagated through all the neurons in the network in order to return the final output. With this in mind, the ultimate goal for a NN is to determine the best value for the weights that maximize the overall accuracy of the predictions [14].

For the network to learn by itself, the weights need to be tuned in order to maximize the accuracy of the network and reduce the loss. For this to be possible, the optimization process that is most used in NN is the Stochastic Gradient Descent (SGD), where is calculated the partial derivative of the loss relatively to each weight [14]. The partial derivative gives the algorithm an understanding on how to adjust the value of the weights. A negative partial derivative indicates the direction making it closer to the minimum of the function [15]. Additionally, for all of the weights across the network to be updated, it is used a process called backpropagation. In this process, the values of the weights are propagated backwards in the network to update the values and calculate the loss function for each weight [14], [15].

Moreover, networks with more than three layers are referred to as Deep Neural Networks (DNNs) [14], [16]. Although these types of networks are much more complex in comparison with other conventional NNs, they are capable of learning a greater number of features with a higher level of abstraction [14].

2.9.1. Supervised and Unsupervised Learning

There are two main types of learning in the field of Deep Learning: Supervised and Unsupervised Learning.

The goal of Unsupervised Learning is to find patterns in the information that it is given, without labelling the data [14]. This makes it ideal for exploratory data analysis, as the algorithm learns without explicit human guidance [17], [18].

On the other hand, Supervised Learning can be described as a type of machine learning where the datasets are labelled [14] in order to improve the accuracy of the algorithm. In this method, during the neural network training process, the output of the neural network is constantly compared with the labelled data in order to adjust the weights more reliably [15].

2.9.2. Convolutional Neural Networks - CNNs

One type of neural networks are Convolutional Neural Networks (CNNs), which are formed by convolutional layers. This type of networks is designed to process data from multiple arrays such as images [15], since each layer generates a higher level of abstraction. Therefore, as the number of layers increases, the number of features recognised also increases until it is possible to uniquely identify an object [19], [20]. At last, CNNs have four main layers:

- **Convolutional layer** - These layers apply a filter to the considered input and perform a convolution to detect similarities between the two sets of values [20]. Additionally, it is possible to adjust these type of layers using three main hyper-parameters [19]:
 - Number of Filters - Enables the adjustment of the depth of the output in order to improve accuracy;
 - Stride - Specifies the distance of the filter that sweeps across the selected input;
 - Padding - Allows the size of the output to be equal to the size of the input.
- **Pooling layer** - Computes a small set of values and merges them into only one feature [15], thus reducing the number of features in the network [20];
- **Fully-connected layer** - These layers allow for each output node to be connected to a node of the previous layer [19];
- **Rectified linear unit (ReLU) layer** - This activation function sets all negative numbers to zero while maintaining the positive values, for a more efficient training process [20].

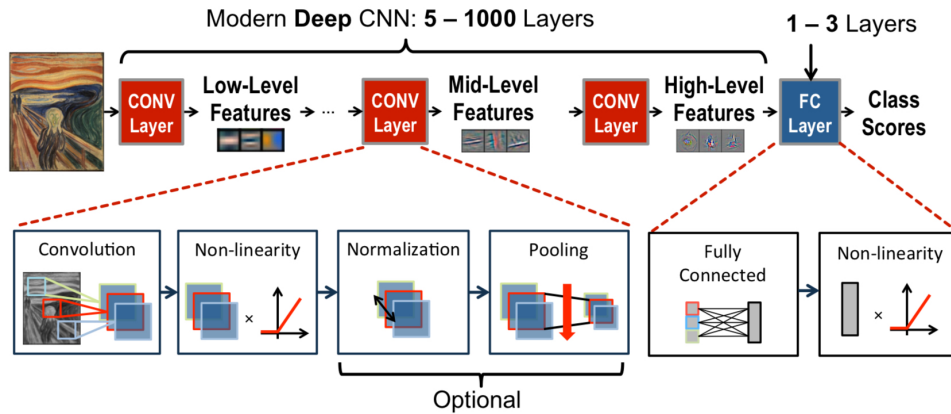


Figure 2.9. Example of a CNN architecture, from [14].

2.9.3. Recurrent Neural Networks - RNNs

Another type of NNs are Recurrent Neural Networks (RNNs), that are characterised for using the feedback connections of past inputs in order to influence the prediction of the current output [21], [22]. Since these networks are designed for data sequences and have the ability to store information about past inputs, they are useful for applications where the input and the output are dependent from each other, such as natural language processing and speech recognition [15], [22], [23].

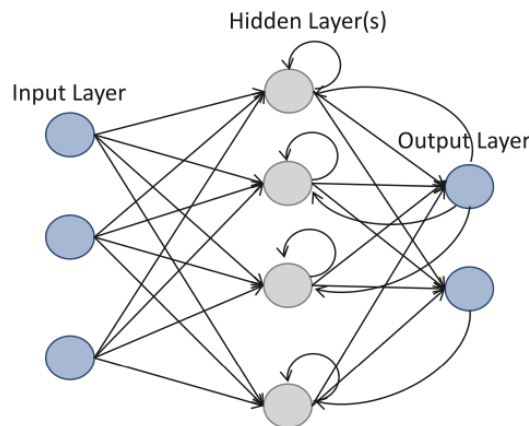


Figure 2.10. Example of a RNN architecture, from [23].

2.9.4. Long Short-term Memory (LSTM) Layers

Long short-term memory (LSTM) layers were firstly introduced in 1997 by Hochreiter and Schmidhuber in [21]. These layers have the ability to learn long-term dependencies between data sequences, thus being appropriate for modeling sequence data [23]. For these structures to have the ability to remember information for a long period of time, they are composed by a memory cell which, at the next time step, has a connection to itself [15].

Moreover, these types of layers rely in three distinct gate units that are responsible for controlling the flow of the information in the LSTM memory cell [24], represented below in figure 2.11. While the update gate (Γ_u) controls how much the unit will be updated, the forget gate (Γ_f) determines the information that the unit forgets. In addition, the output gate (Γ_o) controls the information that is added to the hidden state of the layer. These gate units are all computed with a sigmoid function (σ), which is applied to the current input (a_t) and to the output of the previous timestep (g_{t-1}). Therefore, with these mechanisms, the cell state at timestep t (b_t) is given by

$$b_t = \Gamma_u \otimes \tilde{b}_t + \Gamma_f \otimes b_{t-1} , \quad (2.3)$$

where \tilde{b}_t denotes the candidate for replacing the memory cell. At last, the output of the LSTM layer at time t is defined as g_t and can be obtained as

$$g_t = \Gamma_o \otimes \tanh(b_t) . \quad (2.4)$$

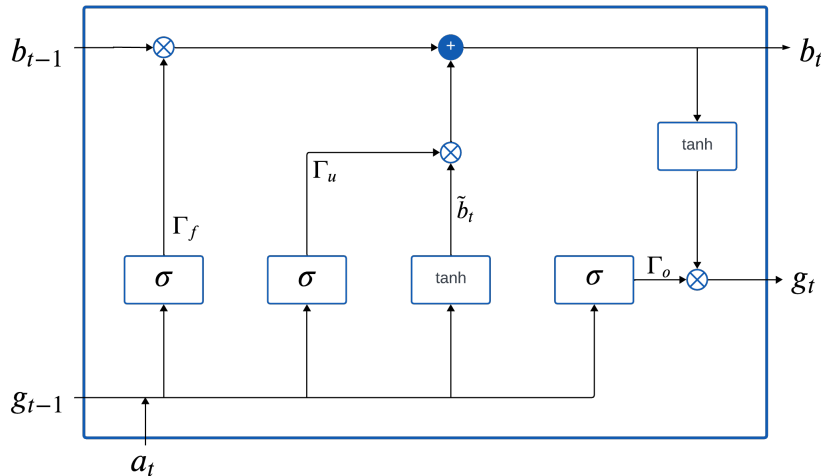


Figure 2.11. Structure of a LSTM unit.

2.9.5. Gated Recurrent Units (GRU) Layers

Gated Recurrent Unit (GRU) layers were proposed in [25] as a low complexity alternative to LSTM layers. Both these types of layers have the ability to learn long-term dependencies between data sequences, however, GRU layers have fewer parameters and a simpler architecture, making them more efficient. Figure 2.12 illustrates the structure of a GRU unit as adopted in this work. This unit relies in two different gate units that depend on the previous hidden state [25]: a reset gate (Γ_r) and an update gate (Γ_u). As the name suggests, the reset gate enables the unit to forget its previous state and the update gate determines how much the unit will be updated [26]. Both these two gates are computed with a sigmoid function (σ), which is applied to the current input (a_t) and to the previous value of the memory cell (b_{t-1}). Moreover, b_t is the output of the GRU unit at time t ,

which is given by

$$b_t = (\tilde{b}_t \otimes \Gamma_u) + ((1 - \Gamma_u) \otimes b_{t-1}), \quad (2.5)$$

where \tilde{b}_t is the candidate activation, which is updated at every timestep.

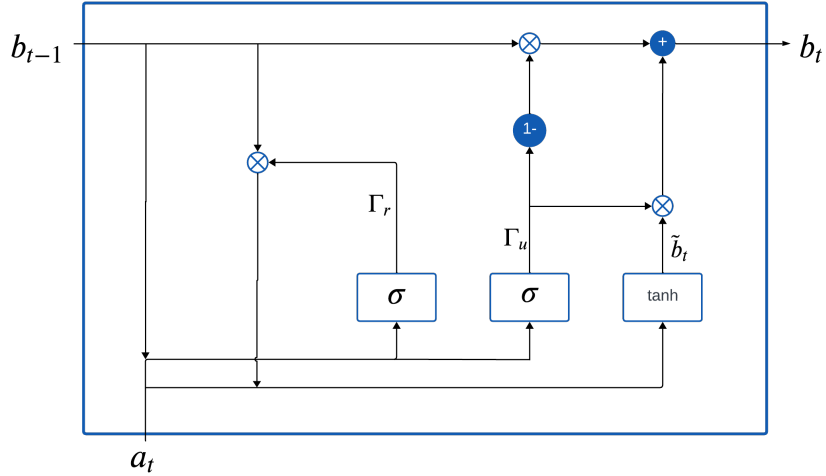


Figure 2.12. Structure of a GRU unit.

2.9.6. Machine Learning applied to MC

The complexity of communication schemes in the Telecommunications domain is increasing considerably. Furthermore, since the detection process is crucial for detecting information that has been sent over a noisy channel, there has been a need to incorporate machine learning techniques for estimating the transmitted information.

Since the molecular channel is very unpredictable due to the random motion of the information molecules (already mentioned in 2.4), the implementation of NNs in the demodulation process is proving to be very successful [27], [28].

The application of one-dimensional CNNs has been the most popular in the field of MC, being proven its efficiency both in [29] and [27]. Furthermore, given that the molecular channel has a memory, there is still a lack of research that takes into account the temporal variation of the molecular channel, where RNNs have the potential to surpass the accuracy of CNNs [27], [29].

DNN-based MC detectors

In order to fulfil the objectives proposed for this investigation, we rely on NN-based detectors for MC. The following chapter describes the system model, the proposed NN architectures and the synchronisation methods considered for all the simulations regarding this study.

3.1. Transmitted Signal

As already mentioned in section 2.8.1, CSK is a low complexity concentration-based modulation technique where the information is conveyed in the concentration of the information molecules. Hence, each time slot corresponds to one symbol. For this to be possible, the transmitter must change the concentration of molecules over each discrete time slot. For this investigation, we consider a Binary Concentration Shift Keying (BCSK) modulation technique that relies upon the fact that one symbol is represented by a single bit. In its simplest form, bit '1' corresponds to the release of a specific amount of molecules in the molecular channel. On the other hand, bit '0' corresponds to not releasing any information molecules. This specific modulation scheme is called On-Off Keying (OOK) and it is represented in figure 3.1, presented below.

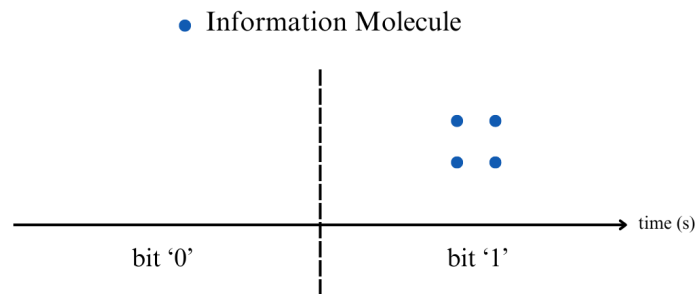


Figure 3.1. OOK modulation scheme, adapted from [4].

In communication systems, synchronisation is required for establishing a link between the transmitter and the receiver. In this work, we assume that a short synchronisation code is employed to ensure that the transmitter and receiver are synchronised. This code consists of a block of known symbols appended to the beginning of the information sequence, in order for the receiver to accurately detect the start of the frame sent by the

transmitter. In this work, we consider the adoption of Barker Codes due to their good autocorrelation properties. In addition, we can append some '0' bits to the considered Barker Code to act as a waiting delay and reduce interference between the synchronisation code and the information frame, thus resulting in a modified Barker Code. Figure 3.2 illustrates the frame structure where N_{BC} represents the length of the modified Barker Code and N_S denotes the number of information symbols.

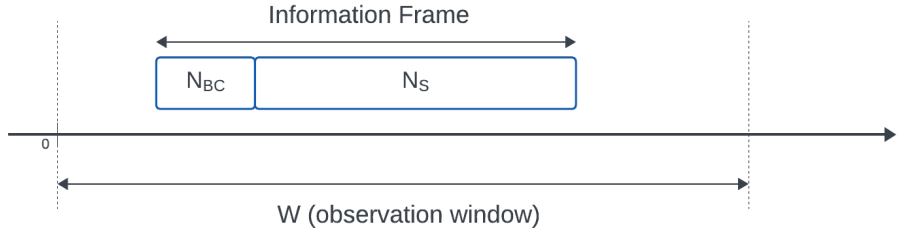


Figure 3.2. Frame structure.

3.2. Signal Pulse Type

For the work proposed in this dissertation, we consider the transmission of information using unipolar Non-return-to-zero (NRZ) pulses over the molecular channel. The employment of this type of pulses is beneficial when using a BCSK modulation technique, as in this case.

With the combination between this type of signal pulse and modulation technique, when the concentration of information molecules is higher than the threshold, the molecular receptor will consider it to be a bit '1', otherwise, it will consider it to be a bit '0'. In figure 3.3, presented below, it is possible to observe the operation of this type of signal for a more comprehensive understanding.

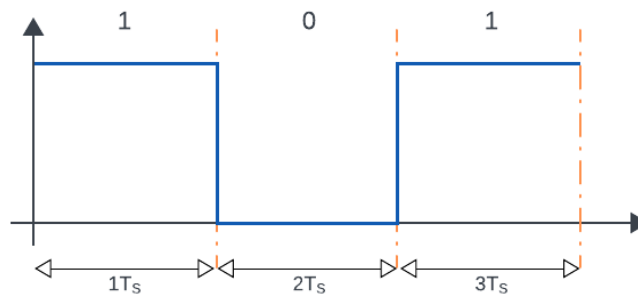


Figure 3.3. Unipolar NRZ pulse.

3.3. Channel Model

To fulfil the objectives proposed in this dissertation, we assume a molecular transmission from a point transmitter to a fully-absorbing receiver. As already mentioned in section 2.6, the model of a point transmitter considers the transmitter as a one-dimensional point where N_{molec} molecules are generated instantaneously, thus not taking into account either the geometry or the effects of the release of the molecules. Moreover, the model of a fully-absorbing receiver assumes that N_{rx} molecules are absorbed by the receiver's membrane during an observation window $[t_u, t_l]$, taking the geometry of the receiver into account. With this in mind, the probability of an information molecule released at time $t = 0$ being absorbed by the molecular receiver at time t during the observation window can be obtained as [13]

$$F_{hit}(t_u - t_l) = \frac{a_{rx}}{d_0} \left[\operatorname{erfc} \left(\frac{d_0 - a_{rx}}{\sqrt{4Dt_u}} \right) - \operatorname{erfc} \left(\frac{d_0 - a_{rx}}{\sqrt{4Dt_l}} \right) \right], \quad (3.1)$$

where $\operatorname{erfc}()$ is the complementary error function, a_{rx} represents the radius of the considered receiver, D denotes the diffusion coefficient, already described in (2.2) and d_0 is the distance between the centre of the transmitter and the centre of the receiver.

Assuming a time-invariant channel, we can define $\bar{h}[t, \tau]$ as the expected number of molecules absorbed at time t by the receiver, after a release of N_{molec} molecules at time τ .

$$\bar{h}[t, \tau] = N_{molec} F_{hit}(t, \tau). \quad (3.2)$$

Then, assuming a Poisson distribution model, we can model the concentration of information molecules released at time t and absorbed by the receiver at time interval τ using

$$h[t, \tau] \sim \text{Poisson}(\bar{h}[t, \tau]). \quad (3.3)$$

To study the transmission of multiple consecutive symbols, it is important to consider a time-slotted channel where each time slot represents one symbol. Moreover, although (3.3) accurately represents the concentration of information molecules absorbed by the receiver, the high level ISI effect is still yet to be taken into account. Hence, taking this effect into account, it is possible to define the concentration of molecules observed at the k -th symbol as

$$y[k] = \sum_{l=0}^{L-1} h[l, k] x[k-l] + n[k], \quad (3.4)$$

where L is the channel memory length and $x[k]$ represents the k -th symbol modulated with BCSK, thus $x[k] \in [A_0, A_1]$ where A_0 and A_1 represent the level for the bit '0' and '1', respectively. In addition, $n[k]$ represents the concentration of interfering molecules following the same statistical model considered in (3.3), namely $n[k] \sim \text{Poisson}(\bar{n}[k])$.

At last, it is possible to define the concentration of information molecules observed by the receiver as

$$y[k] = \underbrace{\bar{h}[0, k]x[k]}_{\text{signal}} + \underbrace{n[k]}_{\text{environmental noise}} + \underbrace{v[k]}_{\text{diffusion noise}} + \underbrace{I[k]}_{\text{ISI}}, \quad (3.5)$$

where the diffusion noise is modelled as a Poisson random variable whose mean has been subtracted. Hence, this variable is defined as $v[k] \sim \text{Poisson}_0(\bar{h}[0, k]x[k])$. Additionally, $I[k]$ represents the ISI effect and is given by $I[k] = \sum_{l=1}^{L-1} h[l, k]x[k-l]$.

3.4. Signal Detection

The main goal of this work is to develop and study NN-based approaches for non-coherent detection in MC. To evaluate the performance of the proposed NN-based detectors, we compare their performance against a direct non-coherent detection. The block diagram in figure 3.4 and 3.5 illustrates the main steps that are performed inside the receiver in order to obtain the final estimates of the information bits, using the two mentioned approaches.

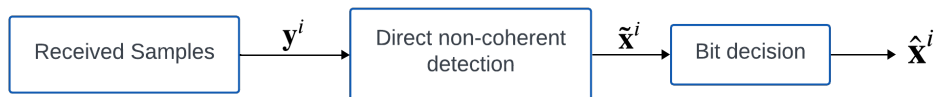


Figure 3.4. Demodulation process for the direct non-coherent detection.

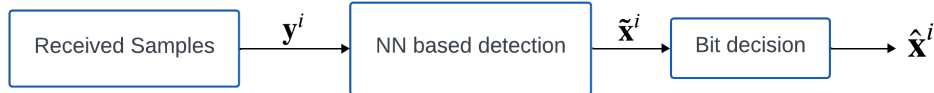


Figure 3.5. Demodulation process for the NN-based non-coherent detection.

3.4.1. Direct Non-coherent Detection

In this work, we consider the adoption of non-coherent detection, which means that the detection process is carried out without any Channel State Information (CSI) estimation. In the case of a conventional non data-driven approach as illustrated in figure 3.4, we apply a direct non-coherent detection to the received samples and, afterwards, we perform a hard bit decision to the soft estimates.

For computing soft symbol estimates in the direct non-coherent detector, we follow the previous work in [30]. First we define the number of received molecules in each position of the N_s bits that compose the information block i as $\mathbf{y}^i = (y^i[1], \dots, y^i[N_s])$. Additionally, considering a BCSK modulation scheme, the k -th symbol of information block i is represented by $x^i[k] \in [A_0, A_1], k = 1, \dots, N_s$, where A_0 and A_1 denote the levels for bit '0' and '1', respectively. Then, we define the probabilities $p_{1,k} = P(x^i[k] = A_1 | \mathbf{y}^i)$

and $p_{0,k} = P(x^i[k] = A_0 | \mathbf{y}^i)$ assuming an uniform distribution with bounds y_{min}^i and y_{max}^i , where $y_{min}^i = \min(\mathbf{y}^i)$ and $y_{max}^i = \max(\mathbf{y}^i)$. These probabilities can be computed as

$$p_{1,k} = \frac{y^i[k] - y_{min}^i}{y_{max}^i - y_{min}^i} \quad (3.6)$$

and

$$p_{0,k} = \frac{y_{max}^i - y^i[k]}{y_{max}^i - y_{min}^i} . \quad (3.7)$$

Using these probabilities it is possible to obtain the Log-likelihood ratio (LLR) for each bit as

$$\lambda^i[k] = \log \left(\frac{p_{1,k}}{p_{0,k}} \right) , \quad (3.8)$$

which allows us to rewrite (3.6) as

$$p_{1,k} = \frac{1}{1 + e^{-\lambda^i[k]}} . \quad (3.9)$$

Bearing in mind that soft values are the conditional expected value of the received symbols, these can be calculated as

$$\tilde{x}^i[k] = E(x^i[k] | \mathbf{y}^i) = (A_1 - A_0)p_{1,k} + A_0 . \quad (3.10)$$

Finally, using (3.9), we can rewrite the expression for the computation of soft estimates as

$$\tilde{x}^i[k] = \frac{(A_1 + A_0)}{1 + e^{-\lambda^i[k]}} + A_0 . \quad (3.11)$$

For OOK, we have $A_0 = 0$ and $A_1 = 1$, therefore (3.11) can be reduced to

$$\tilde{x}^i[k] = \frac{1}{2} \left(\tanh \left(\frac{\lambda^i[k]}{2} \right) + 1 \right) . \quad (3.12)$$

Although we do not consider here in this investigation, these soft symbol estimates can be used as input for a channel decoder when channel coding is employed. Since in this work we assume the transmission of uncoded information, we apply a hard decision to the soft estimates coming from the direct non-coherent detector. Therefore, the k -th estimated bit of information block i , $\hat{x}^i[k]$, can be obtained as

$$\hat{x}^i[k] = \begin{cases} 0, & \tilde{x}^i[k] \leq \phi \\ 1, & \tilde{x}^i[k] > \phi \end{cases} , \quad (3.13)$$

where ϕ represents the threshold value and is given by $\phi = (A_0 + A_1)/2$. In the case of OOK, to map the estimated soft bits into bits '0' and '1', the threshold value becomes $\phi = 0.5$.

3.4.2. Neural Network Based Detection

As an alternative to the direct non-coherent detection, described above in section 3.4.1, we propose a data-driven approach based on the implementation of NNs at the receiver. These NN architectures were firstly aimed at non-coherent detection assuming that the

transmitter and the receiver are synchronised. However, as explained later in this investigation, their design was also extended for scenarios where there is no prior synchronisation between the transmitter and the receiver. Therefore, the proposed NNs in this work are able to accomplish both synchronisation and non-coherent detection in MC.

As it can be observed in figure 3.5, in this approach we apply a NN to the received samples in order to predict the information that was sent through the molecular channel. Similarly to the direct non-coherent detection, the adopted NN architectures output "soft" symbol estimates. Therefore, we apply hard bit decision to map these estimates into bits '0' or '1' using (3.13).

For this investigation, all the proposed NNs were trained considering the same training parameters. Furthermore, all the data for the training process was generated through Monte Carlo simulations. Hence, we used a training dataset (N_{seq}) and a validation set of 19200 sequences, both with $N_s = 20$ bits per frame. However, considering the large quantity of data samples, we divided the dataset into batches of 32 sequences. This method of dividing the dataset in multiple fragments of a smaller size not only reduces overfitting but it also increases the performance and the accuracy of the NN itself. Moreover, the mean square error loss function was adopted, which is described as

$$L_{MSE}(\theta) = \frac{1}{N_{seq}} \sum_{i=1}^{N_{seq}} (f_{\theta}(\mathbf{y}^i) - \mathbf{x}^i)^2, \quad (3.14)$$

considering the NN as a function $f(\theta)$, where θ represents the learnable parameters. Additionally, \mathbf{y}^i and \mathbf{x}^i represent the i -th block of received molecules and information symbols, respectively. Furthermore, the Adaptive Moment Estimation (Adam) method [31] is used as the optimisation algorithm, with an initial learning rate of 0.001. A maximum of 80 epochs were considered, meaning that, during the training process, it will occur 80 full passes through the entire dataset. Additionally, to prevent overfitting, the training data is shuffled before each epoch. At last, we consider a validation patience of 5, meaning that if after five attempts the loss function has not decreased its value, the training progress is stopped.

It is important to note that, following some experiments, it was decided to train all the proposed NNs considering 100 dB in terms of signal to noise ratio (SNR), which is defined as N_{molec}/σ_n where σ_n^2 denotes the noise variance. This choice relies upon the fact that, when trained for a higher N_{molec}/σ_n value, the NNs present a better BER for values of 30 dB and higher. Moreover, all the results presented in this work are obtained from simulations considering a range of N_{molec}/σ_n (per information bit) between 0 dB and 80 dB. At last, it is important to mention that the training of the proposed NNs and the results of the simulations presented in this work were all performed in a system equipped with 48 GB of RAM and an AMD Ryzen 7 1700, which is an 8-core processor with a base clock speed of 3.00 GHz.

Prior to the design of the NN architectures that will be considered in this work, it is necessary to determine whether they should be developed as regression or classification networks. Consequently, we start by designing two different One-dimensional (1-D) convolutional neural networks: one as a regression network and another as a classification network. Table 3.1 and 3.2, presented below, provide a detailed description of the architectural configuration of these NNs, as well as each layer parameters.

Both these NNs share a similar configuration, comprising three 1-D convolutional layers, with a ReLu activation function between each layer. In this case, each 1-D convolutional layer has a stride of 1 and a padding value such that the output sequence matches the size of the input, to ensure consistency in the size of the information frames across all the layers of the network. As for the input, in both NNs, it is implemented a sequence input layer with a "rescale-zero-one" data normalization, to ensure that the input is rescaled to be in the range between 0 and 1. As for the output layer, for the regression NN we included a fully-connected layer, whereas for the classification NN it is adopted a fully-connected layer followed by a softmax layer.

Layer	Type	Filter size	Filters	Activation	Learnable Parameters
1	Sequence input	–	–	–	–
2	1-D Convolutional	9	4	ReLu	40
3	1-D Convolutional	5	2	ReLu	42
4	1-D Convolutional	3	1	ReLu	7
5	Fully-connected	–	–	–	2

Table 3.1. Regression neural network architecture.

Layer	Type	Filter size	Filters	Activation	Learnable Parameters
1	Sequence input	–	–	–	–
2	1-D Convolutional	9	4	ReLu	40
3	1-D Convolutional	5	2	ReLu	42
4	1-D Convolutional	3	1	ReLu	7
5	Fully-connected	–	–	–	4
6	Softmax	–	–	–	–

Table 3.2. Classification neural network architecture.

To evaluate the performance of both the proposed regression and classification NNs for non-coherent detection in molecular communication, we simulate a molecular transmission of 10000 frames of $N_s = 20$ bits assuming perfect synchronisation between the transmitter and the receiver. In this simulation, the BER of both NNs was compared with a direct

non-coherent detection, as previously described in section 3.4.1. The results of this testbed are illustrated in figure 3.6, presented below.

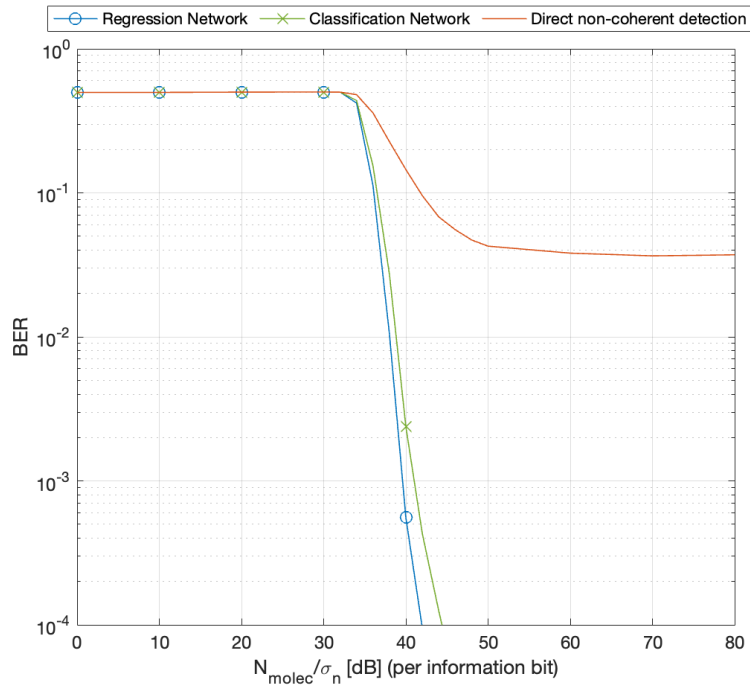


Figure 3.6. BER comparison between the regression and the classification network.

As it can be observed in figure 3.6, both NNs present a similar behavior. However, it is noticeable a slight difference in the performance of the NNs, with the regression network being faster to complete the entire testbed, with a total runtime of 524.5 seconds. In contrast, the classification network required approximately 544 seconds to complete the same simulation.

Given that the molecular channel is very noisy and can be constantly changing, the received signal can vary considerably. Therefore, since the results illustrated in figure 3.6 demonstrated that there is no significant difference between a classification and a regression NN, to address this challenge, in this work we adopted regression networks. This choice relies upon the fact that, with regression networks, it is possible to obtain "soft" bit estimates, which are relevant for a channel decoder when the transmitted information is encoded. However, it is noteworthy that all the architectures adopted in this work can be easily adapted to classification based neural networks.

Finally, all the NNs considered in this work were designed in order to achieve a good trade-off between the complexity of the NN and reliability, in terms of BER values achieved, for the molecular transmission. In addition, it is important to note that all the proposed NNs present a similar number of learnable parameters to ensure a fair comparison between them. Consequently, in this work we considered three different NN architectures: a One-dimensional convolutional neural network based on dilated causal

convolutional layers (CNN), a low-complexity GRU-RNN and a One-dimensional convolutional neural network combined with a gated recurrent unit based recurrent neural network (CNN-RNN), as detailed next.

3.4.3. Recurrent Neural Networks (RNNs)

Given the complexity constraints regarding MC, as already mentioned in section 1.2, it is important to take into account the complexity of the NNs to be considered in this investigation. In this work, we intend to design and employ a RNN due to its ability to remember past inputs. However, these types of NNs are considerably more complex than CNNs. Consequently, we have conducted a set of simulations in order to determine which RNN architecture is the most suitable for this work. Initially, we developed two different single-layer RNNs with a similar architecture and number of learnable parameters, to ensure a fair comparison between the two. In particular, we developed a Long short-term memory based recurrent neural network (LSTM-RNN) and a Gated recurrent unit based recurrent neural network (GRU-RNN), both comprising a sequence input layer as an input layer, followed by a recurrent layer with 20 hidden units. At last, for both RNNs, it was also adopted a fully-connected layer as the output layer. Table 3.3 and 3.4, presented below, describe the detailed architecture of these RNNs for a more comprehensive understanding.

Layer	Type	Hidden Units	Learnable Parameters
1	Sequence input	–	–
2	LSTM	20	1760
3	Fully-connected	–	21

Table 3.3. Single-layer LSTM-RNN architecture.

Layer	Type	Hidden Units	Learnable Parameters
1	Sequence input	–	–
2	GRU	20	1320
3	Fully-connected	–	21

Table 3.4. Single-layer GRU-RNN architecture.

To compare the performance of the proposed RNNs for non-coherent detection in molecular communication, we simulate a molecular transmission of 10000 frames of $N_s = 20$ bits with prior synchronisation between the transmitter and the receiver, similarly to what was done previously. Figure 3.7 illustrates the results of this simulation, where the considered RNNs are compared with a direct non-coherent detection.

In figure 3.7, we can observe that both NNs present a similar behavior. However, given that GRU layers are less complex than LSTM layers, we compare the single-layer

GRU-RNN, previously proposed, against a low-complexity GRU-RNN, whose detailed architecture is described in table 3.5. This specific low-complexity GRU-RNN comprises a sequence input layer as an input layer, followed by two GRU layers with only 4 hidden units each and a fully-connected layer as the output layer.

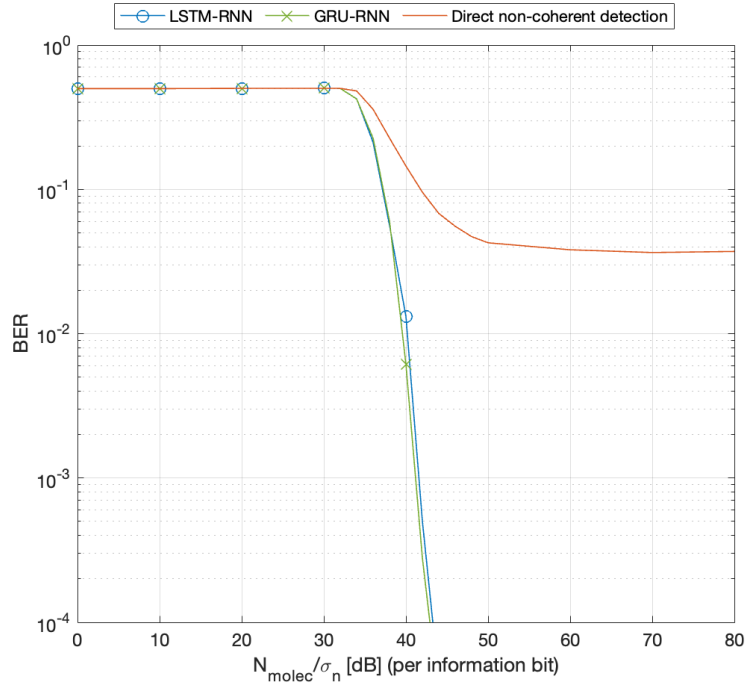


Figure 3.7. BER comparison between the single-layer LSTM-RNN and GRU-RNN.

Layer	Type	Hidden Units	Learnable Parameters
1	Sequence input	–	–
2	GRU	4	72
3	GRU	4	108
4	Fully-connected	–	5

Table 3.5. Low-complexity GRU-RNN architecture.

To compare the performance of these two GRU-RNNs, we follow the same methodology, previously employed for the comparison of the proposed single-layer RNNs. Figure 3.8 illustrates the results of this testbed.

As it can be seen from the results illustrated in figure 3.8, the behaviour of both the proposed GRU-RNNs is very similar. However, it is observed a difference in the elapsed time of the simulations for both scenarios. In this case, the simulation for the low-complexity GRU-RNN required approximately 545 seconds, whereas the single-layer GRU-RNN presented a runtime of 573 seconds.

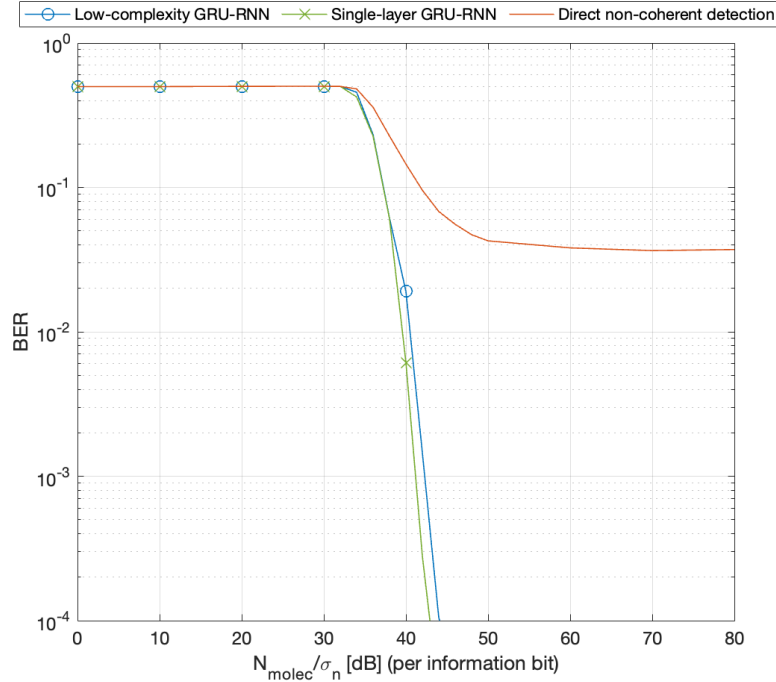


Figure 3.8. BER comparison between the single-layer GRU-RNN and the low-complexity GRU-RNN.

Bearing in mind the previous results regarding to the performance of the aforementioned RNN architectures for non-coherent detection, the low-complexity GRU-RNN revealed to be the most suitable approach. Although the behaviour of the proposed RNNs was very similar, the architecture of the low-complexity GRU-RNN is less complex and is therefore more efficient, requiring a lower runtime in comparison with the other approaches. The block diagram presented in figure 3.10a represents the detailed architecture of this particular GRU-RNN for a more comprehensive understanding. In this case, the input layer receives the sequence data which, subsequently, passes through two GRU layers. This enables the NN to learn long-term dependencies between the sequences that have been processed by the NN. Finally, the information in the NN passes through a full-connected layer, which acts as an output layer, and outputs the "soft" symbol estimates.

3.4.4. 1-D Convolutional Neural Network based on dilated causal convolutional layers (1-D CNN)

CNNs based on dilated causal convolutional layers are a variation of traditional CNNs that have the ability to memorise past inputs [32]. Hence, bearing in mind that the molecular channel has memory, with this NN architecture is possible to take into account the temporal variations of the molecular channel. Specifically, these types of NNs are formed by dilated causal convolutional layers that operate over the discrete time steps of each sequence. Figure 3.9, presented below, illustrates the basic architecture of this NN. Furthermore, one of the main features of these specific NNs is that they are causal, meaning that each current output ($\tilde{x}^i[k]$) does not depend on future inputs [33]. Moreover,

these NNs are formed by convolutional layers with dilation, in order to increase the receptive field of each layer, without increasing the number of parameters. The dilation factor (d_F) determines the step size for sampling the input (\mathbf{y}^i). Consequently, as the dilation factor increases, the distance between two consecutive filter taps also increases. At last, the receptive field (R) is equivalent to the time steps of the input sequence used by the network for each estimate, which is calculated as

$$R = (f - 1)(2^J - 1) + 1 , \quad (3.15)$$

for a stride of 1 and a dilation factor of 2^{j-1} at layer j , where f denotes the filter size and J is the number of convolutional layers in the NN.

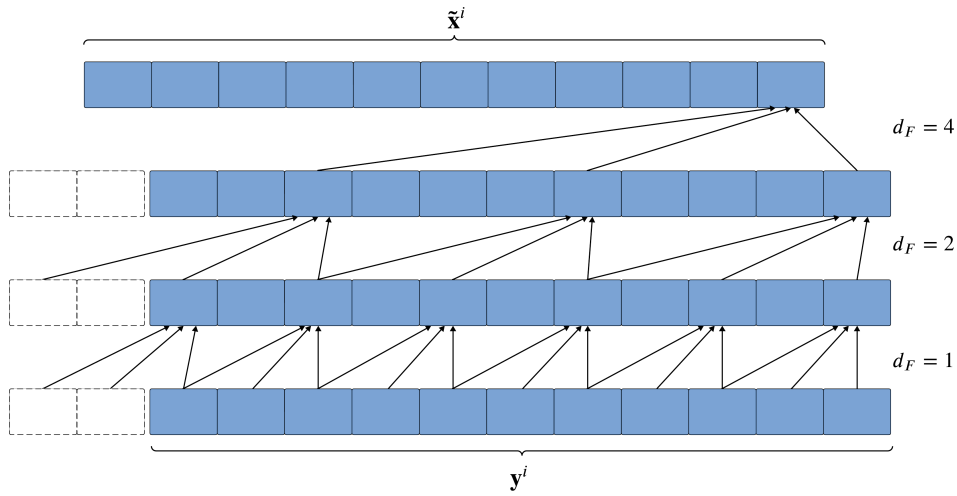


Figure 3.9. Architecture of a 1-D CNN based on dilated causal convolutional layers, adapted from [33].

Layer	Type	Filter size	Filters	Dilation Factor	Activation	Learnable Parameters
1	Sequence input	–	–	–	–	–
2	1-D Convolutional	4	4	1	ReLU	20
3	Batch Normalization	–	–	–	–	8
4	1-D Convolutional	4	2	2	ReLU	34
5	Batch Normalization	–	–	–	–	4
6	1-D Convolutional	4	2	4	ReLU	18
7	Batch Normalization	–	–	–	–	4
8	Fully-connected	–	–	–	–	3

Table 3.6. 1-D CNN based on dilated causal convolutional layers architecture.

In particular, we propose a low-complexity deep NN based on dilated causal convolutional layers, comprising three 1-D convolutional layers with a rectified linear unit (ReLU) activation function and a batch normalization layer between each of these layers. For the input layer, which inputs sequence data to the 1-D CNN, a data normalization is

applied so that the input is rescaled to be in a range between 0 and 1. This network also includes a fully-connected layer as the output layer. Furthermore, each 1-D convolutional layer considers a stride of 1, a filter size of $f = 4$ and a causal method to determine the padding size, which is given by $p = (f - 1)d_F$, to ensure consistency in the size of the frames along the network layers. Moreover, while the first 1-D convolutional layer has 2 filters, the other two have 4 filters. At last, to ensure a larger receptive field, the dilation factor increases exponentially in each convolutional layer, ranging from $d_F = 1$ to $d_F = 4$. In table 3.6, presented below, it is possible to observe the detailed architecture of this NN, as well as the parameters of each layer. In addition, figure 3.10b illustrates the block diagram for this NN architecture.

3.4.5. 1-D Convolutional Neural Network combined with a Gated Recurrent Unit based Recurrent Neural Network (1-D CNN-RNN)

The last NN-based approach corresponds to a NN architecture combining a CNN and a RNN enabling the integration of the aforementioned NNs into a unified solution. In particular, we propose 1-D CNN-RNN, comprising a sequence input layer as an input layer, followed by a 1-D convolutional layer with a ReLu activation function and a batch normalization layer. For the convolutional layer we consider a stride of 1, a filter size of 5 and 2 filters. Furthermore, to ensure consistency in the size of the frames, a causal method is employed to determine the padding size, which is calculated by $p = (f - 1)d_F$, where $d_F = 1$. In addition, we implement a GRU layer with 4 hidden units, followed by a fully-connected layer as the output layer. In table 3.7, it is possible to observe the detailed architecture of this specific NN. In addition, figure 3.10c illustrates the block diagram of its architecture.

Layer	Type	Filter size	Filters	Hidden Units	Activation	Learnable Parameters
1	Sequence input	–	–	–	–	–
2	1-D Convolutional	5	2	–	ReLu	12
3	Batch Normalization	–	–	–	–	4
4	GRU	–	–	4	–	84
5	Fully-connected	–	–	–	–	5

Table 3.7. 1-D CNN-RNN architecture.

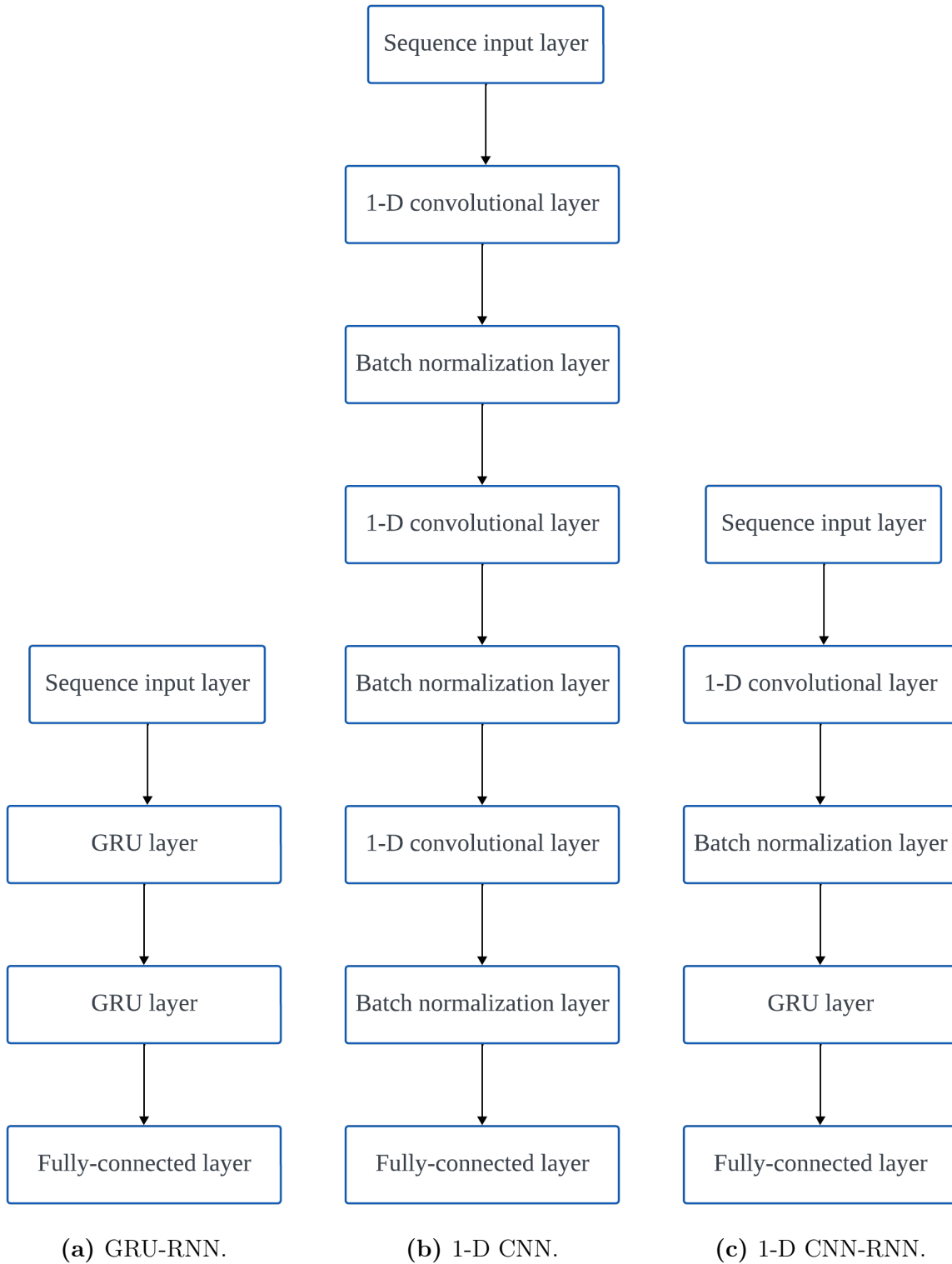


Figure 3.10. Block diagram for each of the proposed NN architectures.

3.5. Frame Synchronisation

For the part of this investigation where we assume a scenario where there is no prior synchronisation between the transmitter and the receiver, we propose three distinct methods

for performing the synchronisation as well as the detection of the information sent from the transmitter to the receiver:

- **Method 1** - In this first method, a NN-based detection is implemented after a conventional synchronisation with the considered modified Barker Codes;
- **Method 2** - The second method relies on the implementation of a NN over the entire observation window of the receiver. Hence, in this case, we accomplish joint synchronisation and detection using a single NN;
- **Method 3** - With this method we propose the implementation of two different NNs, one for the synchronisation and another for the detection process.

Method 1 relies on the implementation of the NNs proposed in 3.4.2 exclusively for the detection process, whereas the synchronisation process is governed by a conventional synchronisation. The demodulation processes that are performed for this method are represented in figure 3.11 in a block diagram.

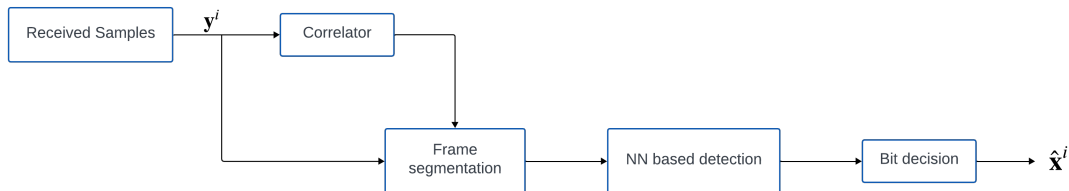


Figure 3.11. Demodulation process for method 1.

The conventional synchronisation relies on correlations between the received signal and the modified Barker Code along the whole observation window. The location of the maximum value for all the performed correlations is assumed to be the position of the synchronisation code in the observation window. Therefore, the position of the beginning of the information frame (\hat{k}_0) can be computed as

$$\hat{k}_0 = \operatorname{argmax}(\mathbf{c}^T \mathbf{y}[k : k + N_{BC} - 1]), \quad 0 \leq k \leq W - N_{BC} - N_s . \quad (3.16)$$

In this case, the bit sequence and the length of the modified Barker Code are represented by $\mathbf{c} = [c_0, \dots, c_{N_{BC}-1}]^T$ and N_{BC} , respectively. In addition, N_s defines the total number of information symbols and W represents the size of the observation window. At last, after obtaining the position of the synchronisation code, a NN is applied to the following 20 symbol positions in order to estimate the information that was received.

As for **method 2**, we follow an approach where a NN similar to the ones proposed in section 3.4.2 is applied to the entire observation window for a joint synchronisation and detection. As it can be observed in figure 3.12, we start by applying a NN to the whole observation window as is done in a NN-based detection, thus obtaining soft bit estimates. Then, we perform a hard bit decision to the predicted result to map the soft estimates into bits '0' or '1', using (3.13). Afterwards, to find the beginning of the information frame, we apply a simple correlation between the estimated sequence and the Barker Code, similarly to (3.16). Finally, knowing the position of the synchronisation code in the observation

window, we segment the frame by extracting the following N_s bits, which are considered to be the information that was sent by the transmitter.

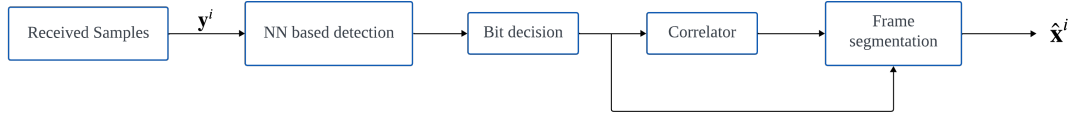


Figure 3.12. Demodulation process for method 2.

Finally, for **method 3**, we propose the implementation of two separate NNs also similar to the ones presented in section 3.4.2: one for the synchronisation and another one for the detection process, as can be observed in figure 3.13. For this to be possible, we start by following an approach similar to method 2. However, in this approach, after the correlation process to detect the beginning of the information frame, we segment the bit sequence \mathbf{y}^i . Afterwards, we apply a NN-based detection to the resulting N_s samples in order to obtain soft bit estimates. Finally, using (3.13), we apply a hard decision to the soft estimates to map them into bits '0' or '1' to detect the information that was sent through the molecular channel.

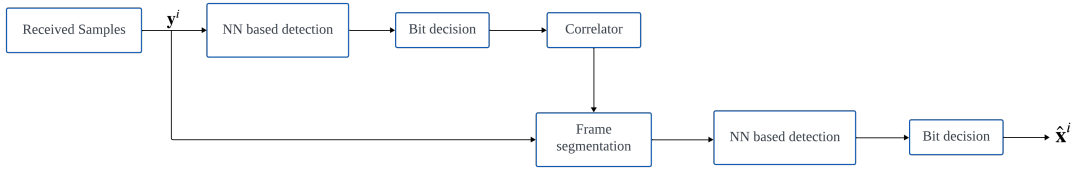


Figure 3.13. Demodulation process for method 3.

Numerical Results

In this chapter, we present the results of the simulations conducted in this investigation, in order to evaluate the proposed NN-based approaches for MC.

4.1. Simulation Parameters

Table 4.1 presents the main parameters considered for the simulations performed in this work. For this investigation, we simulate the transmission of blocks of $N_s = 20$ bits using OOK as a modulation scheme with $A_0 = 0$, $A_1 = 1$ and $N_{molec} = 500$. Moreover, we consider a deterministic model of a point transmitter (tx), a spherical absorbing receiver (rx) and a Poisson distribution as a stochastic model for the channel. Furthermore, all simulations considered in this work assume the transmission of uncoded unipolar NRZ signals where each sample corresponds to a symbol.

Parameters	Values
Molecules transmitted	500
Deterministic model	Point transmitter to Spherical absorbing receiver
Stochastic model	Poisson
Signal pulse type	Unipolar NRZ
Symbol duration (T_s)	$\alpha \cdot \frac{d_{tx-rx}^2}{6D}$ [s]
Modulation scheme	OOK

Table 4.1. Main parameters considered for the Monte Carlo simulations.

Moreover, for the symbol duration (T_s), which has a significant impact on the transmission process, we used

$$T_s = \alpha \cdot \frac{d_{tx-rx}^2}{6D}. \quad (4.1)$$

It is important to note that, for all simulations presented in this paper, we have defined the scaling factor (α) as 1.

Attending (4.1), we can conclude that the diffusion coefficient (D) and the distance between the transmitter and the receiver (d_{tx-rx}) have a direct effect on the assumed symbol duration, which has a major influence on the ISI effect in the communication. Depending on the applications in which molecular communications are envisioned to be deployed, it is possible that the surrounding environment will be constantly changing.

This implies that the transmitter and the receiver may move closer or further apart from each other, resulting in variations in the distance between these two devices. Furthermore, the diffusion coefficient, previously described in (2.2), influences the propagation speed of the information molecules through the molecular channel [13] and directly depends on the temperature and the viscosity of the environment. Thus, a variation in these parameters may change the value of the diffusion coefficient, which also has a significant impact on the transmission process. Since it is assumed that the transmitter and receiver have no knowledge of these variations, T_s is set with the expected distance and diffusion values.

In this investigation, we start always by evaluating the performance of the proposed NNs in a scenario where there are no variations in the distance and in the diffusion coefficient. Hence, we consider a distance between the transmitter and the receiver (d_{tx-rx}) of $10 \mu m$ and a value for the diffusion coefficient (D) of $79.4 \mu m^2/s$. Then, bearing in mind the influence that parameters such as the distance between the transmitter and the receiver and the diffusion coefficient have in the transmission process, we also present the results for a scenario considering variations of these parameters.

4.2. Neural Network based detection with perfect synchronisation

In this section, we simulate a molecular transmission using the NN architectures previously proposed in section 3.4.2, assuming perfect synchronisation between the transmitter and the receiver. In order to study the performance of the proposed NNs, all simulations presented in this section are compared with a direct non-coherent detection, using the approach previously described in section 3.4.1.

The results presented in this work are derived from simulations of a molecular transmission of 10000 frames of $N_s = 20$ bits. Given that the quality of the communication directly depends on the channel conditions, the main objective of this investigation is to evaluate the BER of the conventional molecular transmission in comparison against a molecular communication where a NN-based approach is implemented for non-coherent detection. Figure 4.1, presented below, illustrates the results of the aforementioned simulation.

As it can be seen in figure 4.1, for SNR values above 42 dB, the proposed NNs can achieve BER values lower than 10^{-4} . This is a difference of three orders of magnitude when compared with the BER of the direct non-coherent detection, which has a BER floor value of 10^{-1} . In addition, it is possible to observe that, for all NNs, the value of the BER decreases for a SNR value higher than 30 dB, matching the behaviour of the direct non-coherent detection.

At last, it is important to note that the performance of the proposed NNs is very similar. However, the GRU-RNN exhibits a slight advantage, being faster than both the other considered NNs in the detection process, due to its reduced complexity. For this case, the GRU-RNN presented a runtime of 562s, whereas the 1-D CNN and the 1-D CNN-RNN required 603s and 565s, respectively, to complete the entire testbed.

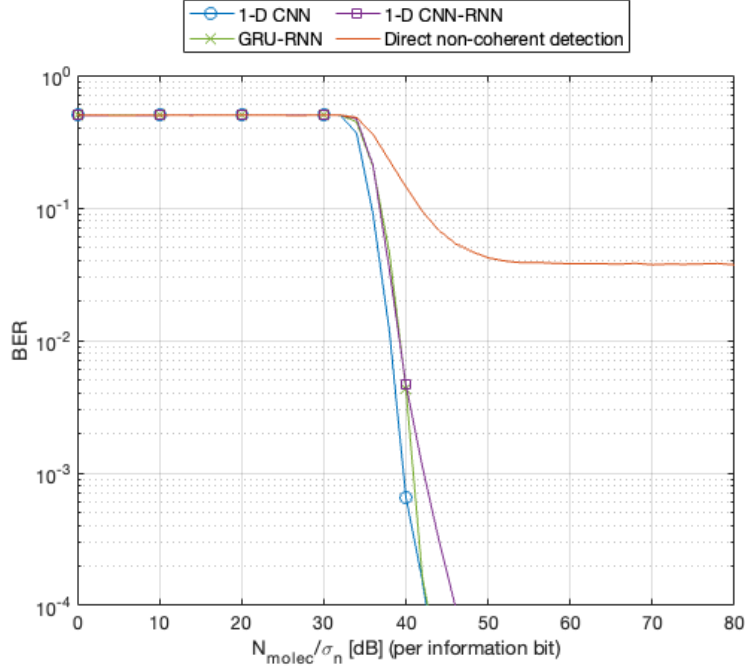


Figure 4.1. BER comparison between the NNs and the direct non-coherent detection.

4.2.1. Distance variations

To evaluate how the proposed NNs perform when there is a variation in the distance between the transmitter and the receiver, we simulated the BER over a range of distances, considering a value of 60 dB in terms of N_{molec}/σ_n . This choice is based on the fact that this parameter strongly influences the channel conditions. Hence, performing simulations with a higher SNR value makes it easier to analyse the results.

For this set of simulations, we considered a scenario where the transmitter and the receiver are moving further apart from each other. Therefore, for this testbed, we chose a range of distances between $5\mu\text{m}$ and $25\mu\text{m}$.

Analysing figure 4.2, it is noticeable that an increase in the distance between the transmitter and the receiver leads to an overall increase of the BER of the molecular transmission.

We observe that, for the 1-D CNN, the BER has a decrease in its value for a small range of distances between $10\mu\text{m}$. This effect is due to the fact that, as already mentioned in 4.1, for this investigation all the NNs are trained considering a distance between the transmitter and the receiver of $10\mu\text{m}$. Therefore, we can conclude that, facing a change in the distance between these two devices, the 1-D CNN only guarantees robustness in the communication for a slight variation in this parameter.

However, the same effect does not apply to the other NN architectures. From the analysis of figure 4.2, we can conclude that, the GRU-RNN, although having been trained with the same parameters as the 1-D CNN, has a better performance over a wider range

of distances, ensuring more robustness facing variations in the distance between the transmitter and the receiver. On the other hand, the BER for the 1-D CNN-RNN starts to increase from a distance value of approximately $14\mu\text{m}$, slightly matching the behaviour of the 1-D CNN.

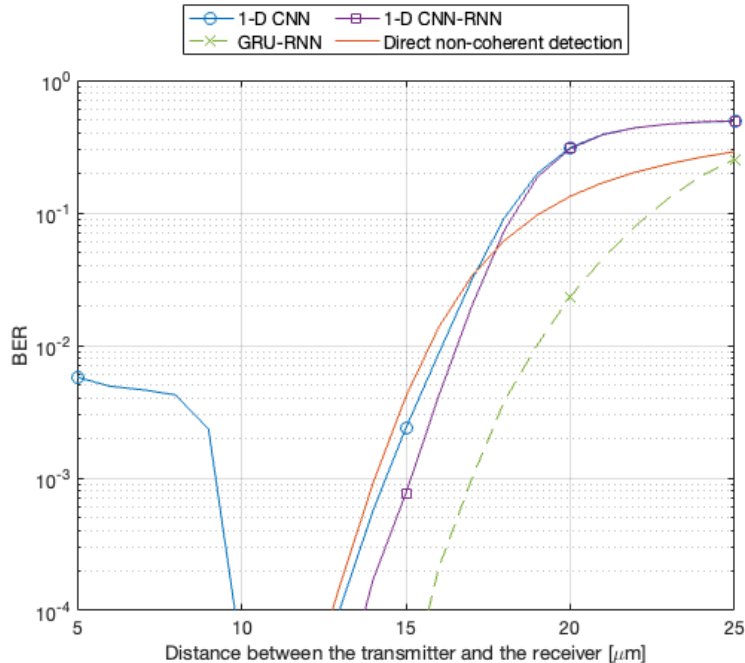


Figure 4.2. BER comparison between the NNs and the direct non-coherent detection for each considered distance value.

4.2.2. Diffusion variations

To test the performance of the proposed NNs facing a scenario where there is a variation in the diffusion coefficient, we simulate the BER of the molecular transmission for an interval of diffusion coefficient errors between -30% and 30% . For this scenario, we consider the same diffusion coefficient used for the training of both NNs (described in 4.1). Moreover, to cope with the expected variations in the molecular channel, we fixed the symbol duration value considering the highest diffusion coefficient error, thus $D_{new} = D + (D \times 0.30)$. In addition, since for a value of 100 dB the BER of the molecular transmission is very low, this complicates the analysis of the results. For this reason, in this case, we considered a value of 40 dB, in terms of N_{molec}/σ_n for these simulations.

From the analysis of figure 4.3, we can conclude that all the proposed NNs are robust for a scenario where there is a variation in the diffusion coefficient. However, it is notable that the 1-D CNN has a significant better performance facing these variations, unlike the other considered NNs. Furthermore, it is possible to observe that the 1-D CNN-RNN has the same behaviour as the 1-D CNN, but with higher BER values. On the other hand, the GRU-RNN is more susceptible to variations in the diffusion coefficient, having a slight decrease in the BER value.

It is important to mention that the BER reduction that can be observed for positive diffusion coefficient values is due to a faster diffusion process. Given that we have considered a fixed value for the symbol duration, this effect of a faster diffusion leads to a reduction in the ISI of the molecular transmission. However, the same does not apply to negative diffusion coefficient errors, where a slower diffusion occurs, thus increasing the ISI effect in the molecular channel.

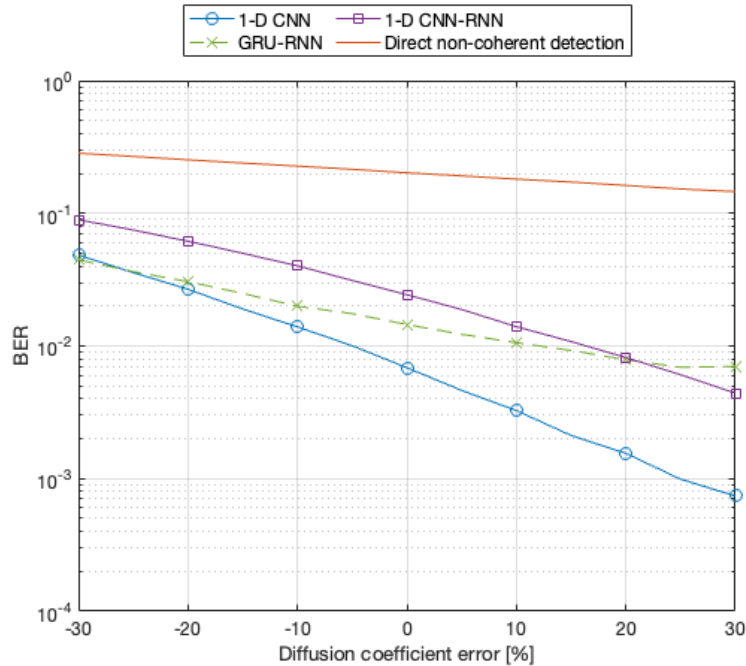


Figure 4.3. BER comparison between the NNs and the direct non-coherent detection for each considered diffusion coefficient error.

4.2.3. Neural Network based detection with perfect synchronisation facing variations in the molecular channel

Taking into account the previous results, we also wanted to evaluate the impact of the variability of the channel conditions and to analyse how to enhance the robustness of the proposed NNs facing this scenario. For this to be possible, unlike the previously presented simulations, we modified the training dataset to include variability in the distance between the transmitter and the receiver and in the diffusion coefficient. Therefore, we simulated the performance of the proposed NNs, trained with a varying range of distances between the transmitter and the receiver and diffusion coefficient errors. For both the validation and the training process, we considered a range of distances between $5\mu\text{m}$ and $15\mu\text{m}$ and diffusion coefficient errors randomly changing between 5% and 15%. In addition, to cope with the expected variations in the molecular channel, which are assumed unknown at the receptor, the symbol duration parameter was modified in order to reduce the ISI effect. Therefore, considering equation 4.1, the parameters considered to define the symbol duration were modified. In this case, d_{tx-rx} is set with a value of $15\mu\text{m}$ whereas

a maximum diffusion coefficient error of 15% was added to the standard value for the diffusion coefficient, resulting $D = 91.31\mu m^2/s$.

In order to study the behavior of the NNs in this scenario, in figure 4.4 we present the results for the original NN architectures, trained both with and without variations in the molecular channel.

Comparing these results with the ones obtained in figure 4.1, we observe an increase in the BER for all NNs, regardless of the training method employed. This can be attributed to the more challenging nature of this scenario, as the considered variations in the distance between the transmitter and the receiver and in the diffusion coefficient lead to a significant deterioration of the molecular transmission, thus increasing the BER.

As it can be seen, training the NNs with variations in the distance and in the diffusion coefficient improves the robustness, leading to a reduction in the overall BER of the molecular transmission for this scenario. We can observe a difference of approximately one order of magnitude when compared with a scenario where no NN is used or where a NN trained without considering variations in these parameters is used.

Finally, we can also observe that, for all the training methods employed, the GRU-RNN has a better performance, achieving a slightly lower BER floor value when compared with the other considered NN architectures. However, it is noticeable that, for 1-D CNN and the 1-D CNN-RNN both trained with variations, the BER starts to decrease from a SNR value of 20 dB, matching the behavior of the direct non-coherent detection. In contrast, for the GRU-RNN, the same does not occur as the BER starts to decrease from a SNR value of approximately 34 dB.

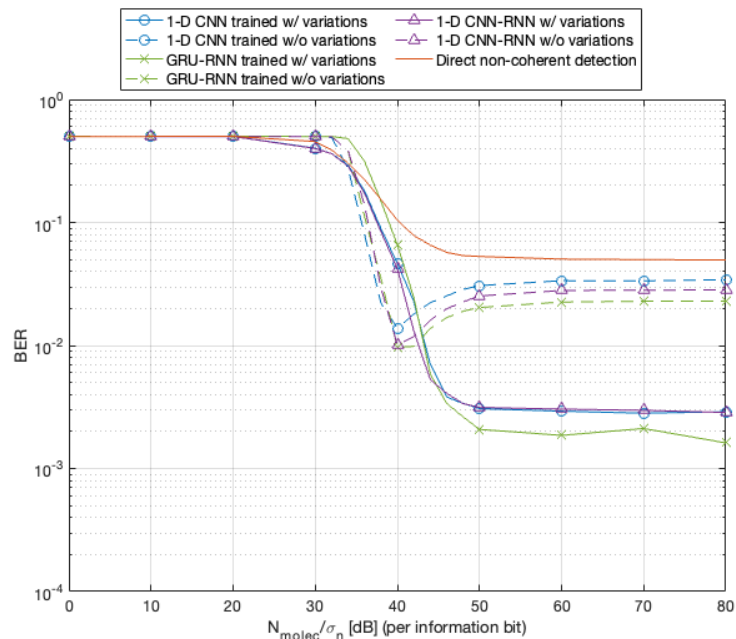


Figure 4.4. BER comparison between the NNs and the direct non-coherent detection, considering variations in the distance and in the diffusion coefficient.

4.3. Neural Networks for the synchronisation and detection process

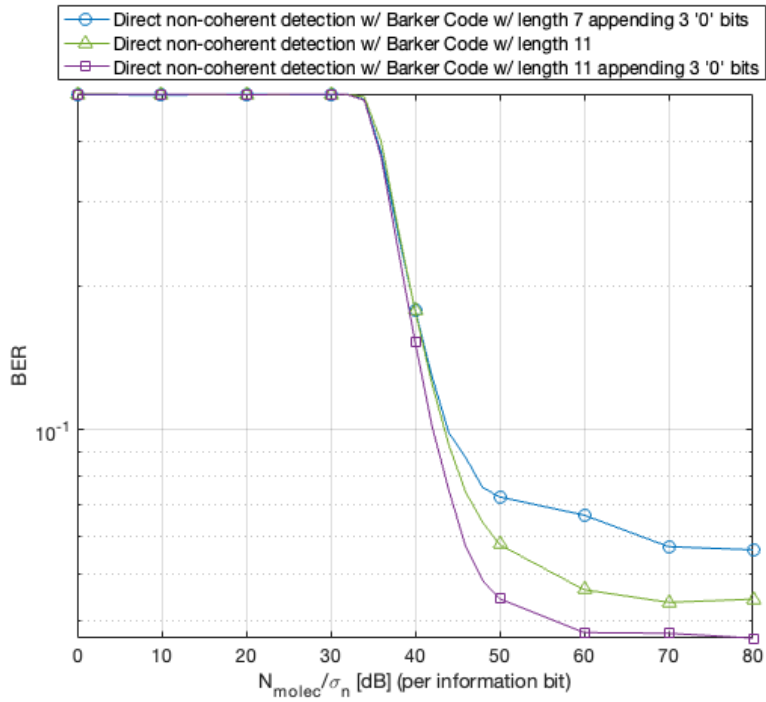
In this section we extend the design of the proposed NNs in order to study their performance for a scenario where there is no previous synchronisation between the transmitter and the receiver. As already mentioned in section 3.1, for this scenario we chose to employ a modified Barker Code for the synchronisation process.

In order to determine the appropriate length of the Barker Code to be employed in this work, several simulations were conducted considering Barker Codes with varying lengths. To provide a concise overview of the study that was conducted, in figure 4.5a and 4.5b we present the BER and the correct synchronisation rate, respectively, for a molecular transmission using a direct non-coherent detection, already described in section 3.4.1, where three distinct types of Barker Codes were employed:

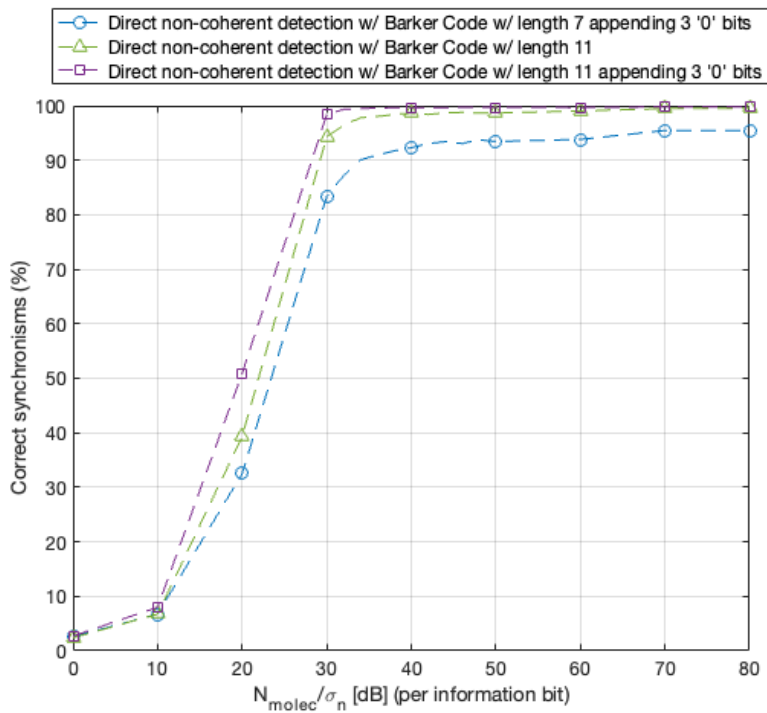
- Barker Code of length 11 - [1 1 1 0 0 0 1 0 0 1 0]
- Modified Barker Code of length 7 appending three additional '0' bits - [1 1 1 0 0 1 0 0 0 0]
- Modified Barker Code of length 11 appending three additional '0' bits - [1 1 1 0 0 0 1 0 0 1 0 0 0 0]

From figure 4.5a, we can observe that, for all the considered Barker Codes, the BER of the direct non-coherent detection exhibits a similar behaviour. As expected, for SNR values above 40 dB, the non-coherent detection employing a longer synchronisation code achieves a slightly lower BER floor value when compared with the other considered Barker Codes. Regarding the correct synchronisation rate, in figure 4.5b we can observe that the longer the Barker Code, the higher is the synchronisation rate. However, the difference between all the considered synchronisation codes is not significant. At last it is important to mention the simulation runtime of the direct non-coherent detection for each of the considered synchronisation codes. The testbed considering a Barker Code with length 7 appending three additional '0' bits required a total runtime of 743s. On the other hand, given that the other synchronisation codes are longer, they are also more complex. Hence, the direct non-coherent detection employing a Barker Code with length 11 presented a runtime of 801s, whereas the simulation considering a Barker Code of length 11 appending three '0' bits required 868s.

Bearing in mind the results obtained previously, the difference between the BER and the correct synchronisation rate for the considered synchronisation codes is not significant. However, the shorter the synchronisation code, the least complex is the synchronisation and the detection process. With this in mind, in this work we consider a modified Barker Code of length 7 appending three additional '0' bits. This choice is based upon the fact that, although this synchronisation code presented slightly higher BER floor values and lower correct synchronism rates, it is the least complex. Hence, this specific Barker Code is a good trade-off between the complexity of the synchronisation process and the highest synchronism rate achieved. Therefore, we consider the following synchronisation binary code: $\mathbf{c} = [1110010000]$.



(a) BER comparison for the direct non-coherent detection for each considered Barker Code.



(b) Synchronisation rate comparison for the direct non-coherent detection for each considered Barker Code.

Figure 4.5. Direct non-coherent detection for the considered Barker Codes.

Regarding the observation window, given that it is assumed that initially the considered molecular receiver only detects an increase in the concentration of the information

molecules, it will not be able to determine whether it detected the end or the beginning of the information frame. Hence, in this work, we consider that the receiver works with an observation window three times larger than the transmitted frame. Therefore, for a frame of $N_s = 20$ bits and a modified Barker Code with a total of $N_{BC} = 10$ bits, the receiver has an observation window of $W = 90$ bits, plus the maximum channel memory length which is considered to be of $L = 7$ symbols.

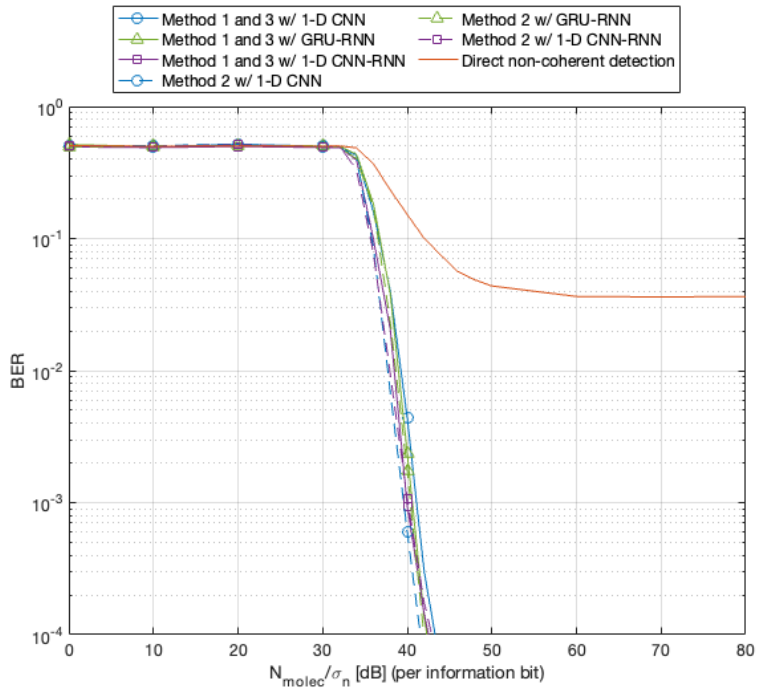
Finally, it is important to mention that all the simulations presented in this section will be compared with a direct non-coherent detection, where no NN is applied.

To evaluate the performance of the NNs for each of the proposed methods, we consider the same parameters and values described in section 4.1. Moreover, we present the results of the BER and the synchronisation rate as a function of N_{molec}/σ_n , in order to observe the evolution of the accuracy of each method. Additionally, it must be noted that the BER results only consider the cases where the synchronism was correct.

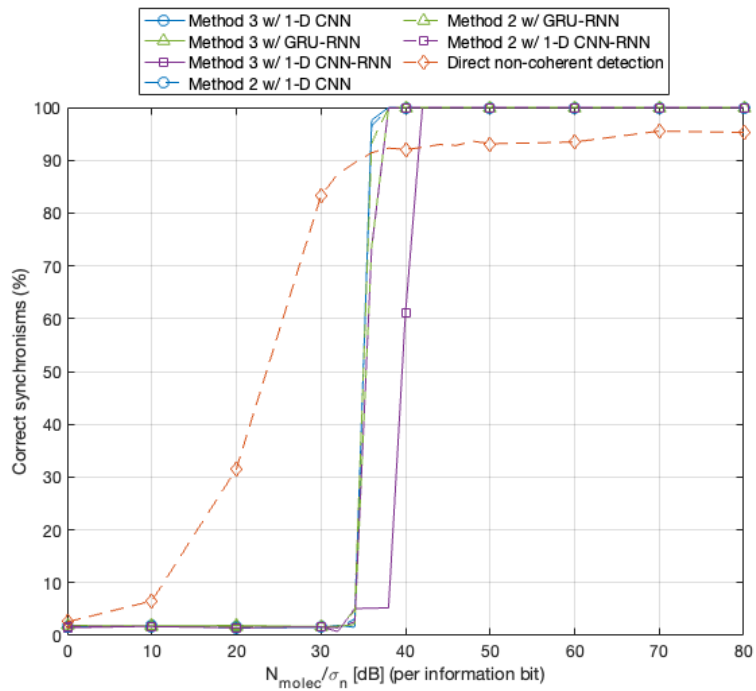
From the analysis of figure 4.6a we can conclude that, for each method, the proposed NNs have a similar behavior. Finally, it is important to mention that, since the detection process is the same for both method 1 and method 3, the results for these methods are illustrated in the same plot line.

As it can be seen in figure 4.6b, since both method 1 and the direct non-coherent detection apply a conventional correlation for the synchronisation process, the result for these two scenarios are illustrated in the same plot line. Moreover, we can observe that, in this case, there is an increase in the rate of correct synchronisms for SNR values between 10 dB and 40 dB, achieving a successful synchronisation rate above 90% for values over 40 dB. Although method 1 shows better synchronisation rates for SNRs below 35 dB, it corresponds to a scenario in which the BER is very high, approaching 50%, therefore making it less relevant. In contrast, for method 2 we can observe synchronisation rates of 100% for values of 40 dB and above for all the proposed NNs. However, for all the NN-based approaches, it is important to note that, for this case, the synchronisation rate only starts to increase at SNRs around 35 dB but it quickly reaches its maximum value, having more consistency in comparison with the direct non-coherent detection. Finally, for method 3, we can observe that the the synchronisation rate is identical for the 1-D CNN and the GRU-RNN achieving synchronisation rates of 100% for values of 40 dB and above. However, for the 1-D CNN-RNN, for a value of 40 dB it is only possible to achieve a successful synchronisation rate of 60%, reaching 100% for SNR values above 42 dB.

In addition, this method has a similar performance to method 2. However, since this method relies in the implementation of two NNs, the synchronisation and detection process incurs in a higher complexity when compared with method 2.



(a) BER comparison between the NNs and the direct non-coherent detection for each method.



(b) Synchronisation rate comparison between the NNs and the direct non-coherent detection for each method.

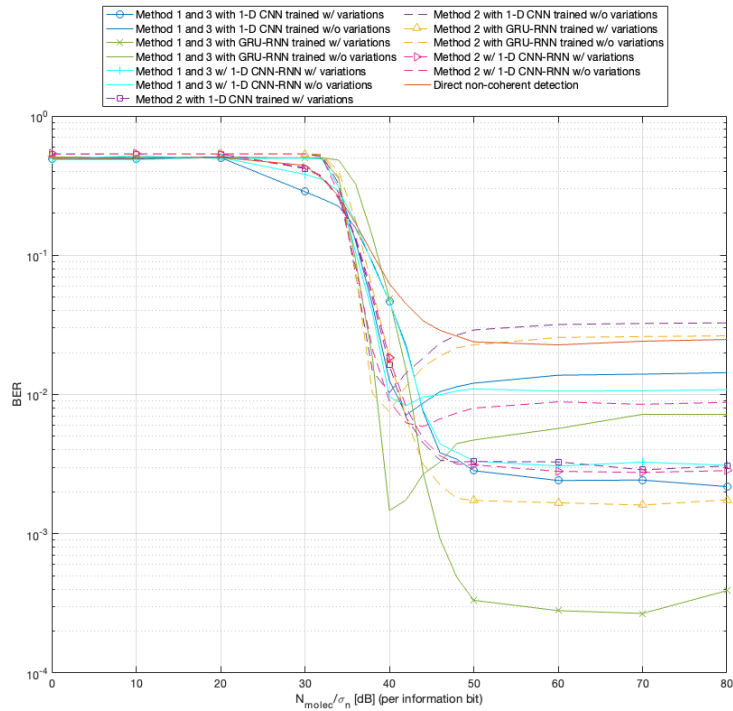
Figure 4.6. NNs applied to each synchronisation and detection method.

4.3.1. Neural Networks for the synchronisation and detection process facing variations in the distance and in the diffusion coefficient

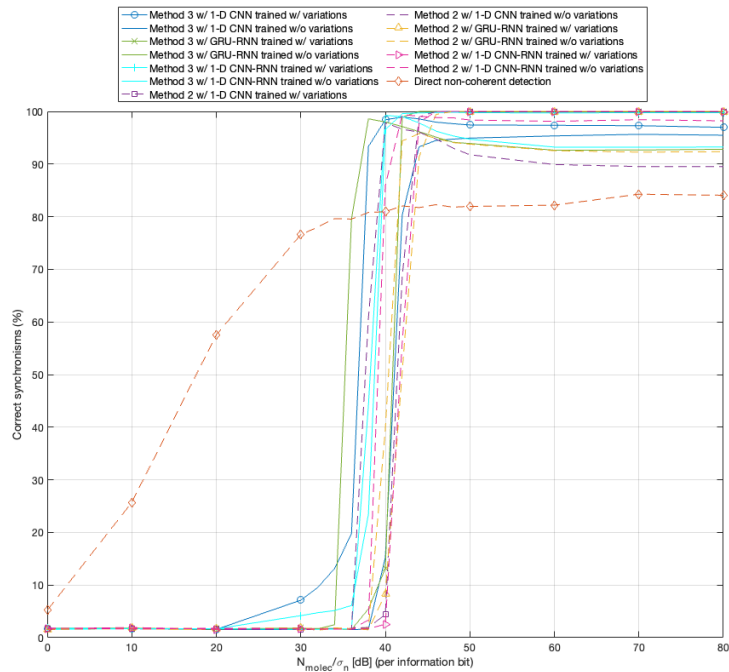
Bearing in mind the previous results, in the following testbed we evaluate the performance of the proposed NNs for each of the previously mentioned methods of synchronism, considering a scenario with variations in the distance between the transmitter and the receiver as well as the diffusion coefficient. For this to be possible, we consider a range of distances between $5\mu\text{m}$ and $15\mu\text{m}$ and diffusion coefficient errors randomly varying between 5% and 15% for both the training and the validation process.

As it can be seen in figure 4.7a, for each of the considered methods, the NNs that were trained considering variations in the distance and in the diffusion coefficient have a better performance, achieving lower BER values when compared with the other scenarios.

Regarding the synchronisation rate, illustrated in figure 4.7b, we can observe a significant reduction in the synchronisation rate for the direct non-coherent detection (and for method 1 since this also implements a conventional synchronisation). Unlike the 90% synchronisation rate achieved previously in 4.6b, in this case it is only possible to achieve a maximum synchronisation rate around 84%. Regarding method 2, unlike what was observed in figure 4.6b, for all NNs trained considering variations in the distance and in the diffusion coefficient, it is only possible to achieve a synchronisation rate of 100% for N_{molec}/σ_n values of approximately 45 dB and above. For method 3, it is possible to observe that the synchronisation rate for the 1-D CNN and for the 1-D CNN-RNN, both trained with variations, starts to increase for SNR values of 20 dB and above. Moreover, it is noticeable that, for GRU-RNN, it is possible to achieve a synchronisation rate of 100% for N_{molec}/σ_n values of approximately 45 dB and above. However, for the 1-D CNN trained with variations, it is only possible to achieve a maximum synchronisation rate of approximately 96%. In contrast, the same does not occur when the proposed NNs are trained without considering variations in the distance and in the diffusion coefficient.



(a) BER comparison between the NNs and the direct non-coherent detection for each method.



(b) Synchronisation rate comparison between the NNs and the direct non-coherent detection for each method.

Figure 4.7. NNs applied to each synchronisation and detection method, considering variations in the distance and in the diffusion coefficient.

Conclusions and Future Work

Molecular Communication has the potential to be at the heart of IoBNT due to its revolutionary capabilities that transcend traditional communication systems. However, the unpredictable nature of the molecular channel induces environment noise and causes high ISI interference, making these two of the main challenges to overcome regarding this type of communication. To help address these problems, in this work we propose a low complexity 1-D CNN based on dilated causal convolutional layers, a low-complexity GRU-RNN and a 1-D CNN-RNN based approach, all aimed at achieving non-coherent detection and synchronisation in MC receivers, in order to increase the robustness of the molecular transmission.

Initially, we described these data-aided NNs-based approaches for accomplishing detection, assuming that the transmitter and the receiver were previously synchronised. For this scenario, it was observed that the proposed NNs perform significantly better when compared with a direct non-coherent detection, with the GRU-RNN having lower complexity and a slightly better performance when compared with the other proposed NNs.

Subsequently, we have extended the proposed NN architectures for scenarios where there is no prior synchronisation between the transmitter and the receiver, proposing two different synchronisation methods. In this part of our study, we have concluded that the implementation of the NNs for the synchronisation process increases the correct synchronisation rate, thus adding greater robustness to the molecular transmission. Moreover, comparing the use of a single NN for joint synchronisation and detection against the use of two separate NNs for synchronisation and detection, it was observed that the later achieves a better performance in terms of BER. However, this is not the case when considering the synchronisation rate, which is very similar for both methods.

Finally, in this work, we also investigated the behaviour of the proposed NNs properly trained for scenarios where there are unknown variations in the distance and in the diffusion coefficient. Given this more challenging setting, it was observed that the proposed NN-based non-coherent detection and synchronisation schemes can provide more robustness than a conventional non-data aided approach.

The present work has resulted in the publication of the research article referenced in [34], which is also included in Appendix A.

5.1. Future Work

Despite the extensive research conducted up to this point regarding MC, this type of communication is still in its infancy. The unpredictability of the MC channel and the high ISI interference represent only a couple of the main challenges that must be overcome in order to achieve a fully functional MC communication system.

In the context of our research, there are certain topics that could be further investigated in order to deepen our knowledge regarding MC systems:

- In this investigation, we considered a OOK as a modulation technique, where one symbol is represented by a single bit. However, other modulation techniques could be investigated so that one symbol could be represented by multiple bits, thus increasing the transmission rate of the information sent through the molecular channel;
- In this work we adopted three distinct NN-based detectors aimed at synchronisation and non-coherent detection. Consequently, an additional investigation considering other low-complexity NN architectures could enhance our understanding regarding NN-based detectors applied to MC;
- Relatively to the scenarios where there is no perfect synchronisation between the transmitter and the receiver, in this investigation we proposed two frame synchronisation methods to be applied at a fully-absorbing receiver. However, another investigation could be conducted considering symbol-timing synchronisation, assuming a model of a passive receiver;
- For the purpose of this investigation, we adopted NN-based synchronisation and detection schemes assuming only one transmitter and one receiver. However, as future work, this approach could be extended for scenarios with Multiple-input Multiple-output (MIMO) schemes, where there are multiple molecular transmitters and receivers operating simultaneously.

References

- [1] S. Lotter, L. Brand, V. Jamali, *et al.*, “Experimental research in synthetic molecular communications - part i,” *IEEE Nanotechnology Magazine*, 2023, ISSN: 19427808. DOI: 10.1109/MNANO.2023.3262100.
- [2] T. Nakano, M. J. Moore, F. Wei, A. V. Vasilakos, and J. Shuai, “Molecular communication and networking: Opportunities and challenges,” *IEEE Transactions on Nanobioscience*, vol. 11, pp. 135–148, 2 2012, ISSN: 15361241. DOI: 10.1109/TNB.2012.2191570.
- [3] I. F. Akyildiz, M. Pierobon, S. Balasubramaniam, and Y. Koucheryavy, “The internet of bio-nano things,” *IEEE Communications Magazine*, vol. 53, pp. 32–40, 3 2015. DOI: 10.1109/MCOM.2015.7060516.
- [4] N. Farsad, H. B. Yilmaz, A. Eckford, C.-B. Chae, and W. Guo, *A comprehensive survey of recent advancements in molecular communication*, 2016. DOI: 10.1109/COMST.2016.2527741.
- [5] Y. Huang, F. Ji, Z. Wei, M. Wen, and W. Guo, “Signal detection for molecular communication: Model-based vs. data-driven methods,” *IEEE Communications Magazine*, vol. 59, pp. 47–53, 5 May 2021, ISSN: 15581896. DOI: 10.1109/MCOM.001.2000957.
- [6] J. M. Jornet and A. Sangwan, “Nanonetworking in the terahertz band and beyond,” *IEEE Nanotechnology Magazine*, 2023, ISSN: 19427808. DOI: 10.1109/MNANO.2023.3262105.
- [7] L. Chouhan and M. S. Alouini, “Interfacing of molecular communication system with various communication systems over internet of every nano things,” *IEEE Internet of Things Journal*, vol. 10, pp. 14552–14568, 16 Aug. 2023, ISSN: 23274662. DOI: 10.1109/JIOT.2023.3273030.
- [8] H. Zhai, Q. Liu, A. V. Vasilakos, and K. Yang, “Anti-isi demodulation scheme and its experiment-based evaluation for diffusion-based molecular communication,” *IEEE Transactions on Nanobioscience*, vol. 17, pp. 126–133, 2 Apr. 2018, ISSN: 15361241. DOI: 10.1109/TNB.2018.2797689.
- [9] M. S. Kuran, H. B. Yilmaz, I. Demirkol, N. Farsad, and A. Goldsmith, *A survey on modulation techniques in molecular communication via diffusion*, 2021. DOI: 10.1109/COMST.2020.3048099.
- [10] M. Kuscü, E. Dinc, B. A. Bilgin, H. Ramezani, and O. B. Akan, “Transmitter and receiver architectures for molecular communications: A survey on physical design with

- modulation, coding, and detection techniques,” *Proceedings of the IEEE*, vol. 107, no. 7, pp. 1302–1341, 2019. DOI: 10.1109/JPROC.2019.2916081.
- [11] *Internet of Things - Worldwide*, Jul. 2023. [Online]. Available: <https://www.statista.com/outlook/tmo/internet-of-things/worldwide#revenue>.
- [12] W. Guo, T. Asyhari, N. Farsad, *et al.*, “Molecular communications: Channel model and physical layer techniques,” *IEEE Wireless Communications*, vol. 23, pp. 120–127, 4 Aug. 2016, ISSN: 1558-0687. DOI: 10.1109/MWC.2016.7553035.
- [13] V Jamali, A Ahmadzadeh, W Wicke, A Noel, and R Schober, “Channel modeling for diffusive molecular communication—a tutorial review,” *Proceedings of the IEEE*, vol. 107, pp. 1256–1301, 7 2019, ISSN: 1558-2256. DOI: 10.1109/JPROC.2019.2919455.
- [14] V Sze, Y. H. Chen, T. J. Yang, and J. S. Emer, “Efficient processing of deep neural networks: A tutorial and survey,” *Proceedings of the IEEE*, vol. 105, pp. 2295–2329, 12 2017, ISSN: 1558-2256. DOI: 10.1109/JPROC.2017.2761740.
- [15] Y. Lecun, Y. Bengio, and G. Hinton, *Deep learning*, May 2015. DOI: 10.1038/nature14539.
- [16] *What is deep learning?* [Online]. Available: <https://www.ibm.com/topics/deep-learning>.
- [17] *What is unsupervised learning?* [Online]. Available: <https://cloud.google.com/discover/what-is-unsupervised-learning>.
- [18] *What is unsupervised learning?* [Online]. Available: <https://www.ibm.com/topics/unsupervised-learning>.
- [19] *How do convolutional neural networks work?* [Online]. Available: <https://www.ibm.com/topics/convolutional-neural-networks>.
- [20] *What Is a Convolutional Neural Network?* [Online]. Available: <https://www.mathworks.com/discovery/convolutional-neural-network.html>.
- [21] S Hochreiter and J Schmidhuber, *Long short-term memory*. 1997. DOI: 10.1162/neco.1997.9.8.1735. [Online]. Available: <https://search.ebscohost.com/login.aspx?direct=true&db=cmedm&AN=9377276&site=eds-live>.
- [22] *What are recurrent neural networks?* [Online]. Available: <https://www.ibm.com/topics/recurrent-neural-networks>.
- [23] Z. M. Fadlullah, F. Tang, B. Mao, *et al.*, “State-of-the-art deep learning: Evolving machine intelligence toward tomorrow’s intelligent network traffic control systems,” *IEEE Communications Surveys and Tutorials*, vol. 19, pp. 2432–2455, 4 Oct. 2017, ISSN: 1553877X. DOI: 10.1109/COMST.2017.2707140.
- [24] A Shrestha and A Mahmood, “Review of deep learning algorithms and architectures,” *IEEE Access*, vol. 7, pp. 53 040–53 065, 2019, ISSN: 2169-3536. DOI: 10.1109/ACCESS.2019.2912200.

- [25] K. Cho, B. van Merriënboer, D. Bahdanau, and Y. Bengio, *On the properties of neural machine translation: Encoder-decoder approaches*, 2014. [Online]. Available: <http://arxiv.org/abs/1409.1259>.
- [26] J. Chung, C. Gulcehre, K. Cho, and Y. Bengio, *Empirical evaluation of gated recurrent neural networks on sequence modeling*, 2014. [Online]. Available: <http://arxiv.org/abs/1412.3555>.
- [27] M. Bartunik, J. Kirchner, and O. Keszocze, “Artificial intelligence for molecular communication,” *it - Information Technology*, vol. 65, no. 4-5, pp. 155–163, 2023. DOI: doi:10.1515/itit-2023-0029. [Online]. Available: <https://doi.org/10.1515/itit-2023-0029>.
- [28] N. Farsad and A. Goldsmith, “Neural network detection of data sequences in communication systems,” *IEEE Transactions on Signal Processing*, vol. 66, pp. 5663–5678, 21 Nov. 2018, ISSN: 1053587X. DOI: 10.1109/TSP.2018.2868322.
- [29] M. Bartunik, O. Keszocze, B. Schiller, and J. Kirchner, “Using deep learning to demodulate transmissions in molecular communication,” *2022 IEEE 16th International Symposium on Medical Information and Communication Technology (ISMICT)*, pp. 1–6, 2022. DOI: 10.1109/ISMICT56646.2022.9828263.
- [30] S. Figueiredo, N. Souto, and F. Cercas, “Low-complexity channel codes for reliable molecular communication via diffusion,” *SENSORS*, vol. 22, pp. 41–41–55, 1 2022, ISSN: 1424-8220. DOI: 10.3390/s22010041. [Online]. Available: <https://search.ebscohost.com/login.aspx?direct=true&db=edsWSC&AN=000741422400001&site=eds-live>.
- [31] D. P. Kingma and J. L. Ba, “Adam: A method for stochastic optimization,” 2015. [Online]. Available: http://www.scopus.com/scopus/openurl/link.url?ctx_ver=Z39.88-2004&ctx_enc=info:ofi/enc:UTF-8&svc_val_fmt=info:ofi/fmt:kev:mtx:sch_svc&svc.citedby=yes&rft_id=info:eid/2-s2.0-85083951076&rfr_id=http://search.ebscohost.com&rfr_dat=partnerID:NnvIuKwx&rfr_dat=md5:1950f6bbec59b02ffe97483e85f0ba44.
- [32] C. Lea, M. D. Flynn, R. Vidal, A. Reiter, and G. D. Hager, “Temporal convolutional networks for action segmentation and detection,” in *2017 IEEE Conference on Computer Vision and Pattern Recognition (CVPR)*, 2017, pp. 1003–1012, ISBN: 1063-6919. DOI: 10.1109/CVPR.2017.113.
- [33] S. Bai, J. Z. Kolter, and V. Koltun, *An empirical evaluation of generic convolutional and recurrent networks for sequence modeling*, 2018. [Online]. Available: <http://arxiv.org/abs/1803.01271>.
- [34] D. Casaleiro, N. M. B. Souto, and J. C. Silva, “Synchronization and detection in molecular communication using a deep-learning-based approach,” *IEEE Access*, vol. 12, pp. 192 539–192 553, 2024. DOI: 10.1109/ACCESS.2024.3519310.

Received 13 November 2024, accepted 13 December 2024, date of publication 17 December 2024,
date of current version 26 December 2024.

Digital Object Identifier 10.1109/ACCESS.2024.3519310



Synchronization and Detection in Molecular Communication Using a Deep-Learning-Based Approach

DUARTE CASALEIRO¹, NUNO M. B. SOUTO^{2,3}, (Senior Member, IEEE), AND JOÃO C. SILVA³

¹Telecommunications and Computer Engineering, Iscte–University Institute of Lisbon, 1649-026 Lisbon, Portugal

²Instituto de Telecomunicações, 1049-001 Lisbon, Portugal

³Department of Information Science and Technology, Iscte–University Institute of Lisbon, 1649-026 Lisbon, Portugal

Corresponding author: Duarte Casaleiro (duarte_casaleiro@iscte-iul.pt)

This work was supported by the Fundação para a Ciência e Tecnologia (FCT), I.P. by project reference UIDB/50008/2020, and DOI identifier <https://doi.org/10.54499/UIDB/50008/2020>.

ABSTRACT The concept of Internet of Bio-Nano Things (IoBNT) has emerged due to its revolutionary possibilities that transcend traditional wireless communication systems. Molecular Communication (MC) arises as a potential centrepiece for this paradigm, enabling applications in challenging environments. However, this type of communication, which often relies on molecular diffusion, suffers from a high inter-symbol interference (ISI), which deteriorates the reliability of the transmission. To cope with the strong ISI as well as the typical short coherence time of the MC channel, this work considers the adoption of a data-driven approach to accomplish non-coherent based detection at the receiver. In particular, we investigate the performance of a low complexity one-dimensional Convolutional Neural Network (1-D CNN) based in dilated causal convolutional layers and of a Gated Recurrent Unit based Recurrent Neural Network (GRU-RNN) aimed at the tasks of symbol detection and synchronisation, comparing the results with a conventional non-coherent detection. Initially, we study the performance of the proposed Neural Networks (NNs) based detectors assuming prior synchronisation between the transmitter and the receiver and, afterwards, we extend the approach for scenarios without prior synchronisation. Furthermore, we also investigate the robustness of the proposed NNs schemes against unknown variations in the distance between the transmitter and the receiver as well as in the diffusion coefficient. Finally, the results presented in this work lead to the conclusion that the implementation of NNs for both synchronisation and non-coherent detection can be a very effective approach for the challenging MC channel, ensuring more robustness than conventional model-based approaches.

INDEX TERMS 6G, future wireless networks, molecular communications, neural networks.

I. INTRODUCTION

Throughout history, the Telecommunications domain has been improving in order to enhance our knowledge, our society and our industries. Currently, the research work regarding to the sixth generation (6G) wireless systems is expected to enable communications in environments previously considered unfeasible [1]. Therefore, to fulfil these challenges, the Internet of Bio-Nano Things (IoBNT) paradigm emerges due to its ability to enable the formation

of networks between bio-devices [2]. Given the extreme environments in which IoBNT is envisioned to be deployed, it is imperative that the devices communicate in a way that does not deteriorate the surrounding environment, so-called biocompatibility.

With this in mind, Electromagnetic Communication (EM) at nanoscale has restrictions since the antenna size is proportional to the signal wavelength [3], [4]. This implies operating in the Terahertz (THz) range [4], [5]. Still, operating at these higher frequency bands, not only increases the attenuation but also emits high-frequency radiation, making it unfeasible for the considered applications in IoBNT [2]. On the other hand,

The associate editor coordinating the review of this manuscript and approving it for publication was Mauro Fadda.

Molecular Communication (MC) has the potential to be at the heart of this paradigm since the information is encoded in the physical properties of the information molecules, which act as carriers [2], [4], [6], [7], [8], [9], preventing any emission of radiation, thus ensuring biocompatibility. Additionally, MC is also energy efficient [4] since the propagation of the information molecules follows the random Brownian motion [3], [7], thus not requiring extra energy for the information to propagate through the molecular channel [4]. Furthermore, given the lack of limitations and regulations regarding to MC [4], it is possible to occupy the totality of the bandwidth. This enables a wide range of applications such as targeted drug delivery, health monitoring, pipeline communications for leak detection and swarm control for search-and-rescue missions [6], [10].

Despite the advantages of MC mentioned above, there are still challenges to overcome regarding these communication systems. One of the main challenges is the fact that the molecular channel has memory [3], [8], [9], which means that molecules are slowly absorbed by the molecular receivers [3], [8], remaining in the channel for a random period of time. This causes molecules from previous symbols to interfere with molecules from the current symbol, leading to a high inter-symbol interference (ISI) [4], [8], which restricts the transmission rates. Additionally, the scale and the environments in which MC communications systems are envisioned to be deployed require low complexity modulation, coding and detection schemes, while still ensuring robustness in the communication.

Similarly to traditional communication systems, MC systems are composed by a transmitter, a receiver and a channel through which the information is conveyed [4]. Relatively to the transmission process, it can be characterised as passive [10], where the information molecules propagate through the molecular channel via diffusion, or as propulsive [10], where the propagation of the molecules is induced by external forces, requiring extra energy. Regarding the propagation in the molecular channel via diffusion, it is one of the most studied methods due to its simplicity. In this type of MC, the information molecules propagate through the molecular channel, introducing a certain level of randomness into the channel itself. This implies that the molecular channel is constantly changing, making it difficult to estimate [11]. As for molecular receivers, they can be passive [9], where molecules are observed in an indirect form which does not change the concentration of molecules, or absorbing [9], where the molecules are absorbed and removed from the molecular channel. In order to encode the information in the physical properties of the molecules, there are several modulation schemes available. However, concentration shift keying (CSK) has been the most studied given its low complexity, since the information is encoded in the concentration of the information molecules [3].

Given the complexity constraints of MC, a non-coherent detection can be a solution for the detection process due to its simplicity [4] since this type of approach does not

require the estimation of channel state information (CSI) of the molecular channel [11]. Additionally, in MC, data-driven detectors can potentially have a better performance than model-driven ones [4]. Against this background, non-coherent detection based on a data-driven approach using a low-complexity neural network (NN) can be beneficial when the characteristics of the molecular channel are unknown [4].

Moreover, the implementation of neural networks in the demodulation process is proving to be very successful [12], [13]. Both in [12] and [14] it was shown the efficiency of convolutional neuronal networks (CNNs) in MC systems in order to decode the information sent through the inherently noisy molecular channel. These types of NNs are formed by convolutional layers, each one generating a higher level of abstraction, in order to extract essential information from the input [15]. For this to be possible, a filter of a given size sweeps across the input performing several convolutions. As already mentioned, the molecular channel has memory. Therefore, recurrent neural networks (RNNs) have the potential to surpass the accuracy of CNNs [12], [14]. This is due to the fact that RNNs use the feedback from past inputs to predict the current output [4], [16], thus taking into account the temporal variations of the molecular channel.

Based on the work and concepts mentioned above, in this paper we investigate the implementation of low complexity NNs in MC receivers, which can accomplish synchronisation and non-coherent detection of the MC signal. In order to demonstrate the effectiveness of the proposed NN architectures, we rely on extensive Monte Carlo simulations to evaluate the bit error rate (BER) of the molecular transmission. The main objective is to achieve a NN with reduced implementation complexity, while ensuring robustness in the communication itself. The main contributions presented in this research paper are the following:

- 1) We propose both a low complexity one-dimensional convolutional neural network (1-D CNN) based on dilated causal convolutional layers and a gated recurrent unit based recurrent neural network (GRU-RNN) architecture, which can perform non-coherent molecular detection, assuming prior synchronisation between the transmitter and the receiver.
- 2) We extend the design of the proposed 1-D CNN and GRU-RNN based approaches for scenarios where there is no previous synchronisation between the transmitter and the receiver. Two different methods are presented. One relies on two separate NNs dedicated to the synchronisation and detection tasks, whereas the second adopts a single NN for accomplishing simultaneous synchronisation and detection.
- 3) We train the proposed 1-D CNN and GRU-RNN based synchronisation and detection schemes in order to enhance their robustness against unknown variations in the distance between the transmitter and the receiver as well as in the diffusion coefficient. It is shown that both NN architectures achieve better performance than conventional non data-aided approaches.

At last, regarding its structure, this paper is organised as follows:

- In section II we introduce the considered system model.
- In section III, we present a description of the proposed architectures adopted for the neural networks, as well as the methods considered for synchronisation.
- Section IV describes the numerical simulations carried out for evaluating the performance of the different approaches.
- Section V presents a summary of the key conclusions obtained with this investigation.

II. SYSTEM MODEL

A. TRANSMITTED SIGNAL

In MC, the modulation process consists of encoding the information in the physical properties of the information molecules. As described in [9], there are several types of modulation techniques such as concentration-based, type-based, timing-based and spatial-based. Additionally, it is also possible to have hybrid techniques that rely on the combination of two or more modulation schemes.

CSK is a concentration-based modulation technique where the information is conveyed in the concentration of the information molecules. For this to be possible, the transmitter must change the concentration of molecules over each discrete time slot. In this paper, we consider a Binary CSK (BCSK) modulation technique that relies upon the fact that one symbol is represented by a single bit. In its simplest form, bit '1' can correspond to the release of a specific amount of molecules and bit '0' can correspond to not releasing any molecules. This specific modulation form is called On-Off Keying (OOK) and is represented in figure 1.

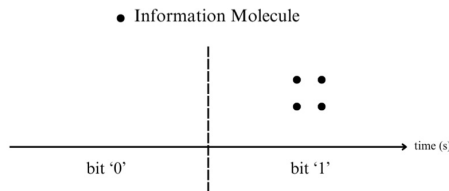


FIGURE 1. OOK modulation scheme, adapted from [3].

In communication systems, synchronisation is required for establishing a link between the transmitter and the receiver. In this work, we assume that a short synchronisation code is employed to ensure that the transmitter and receiver are synchronised. This code consists of a block of known symbols appended to the beginning of the information sequence, in order for the receiver to accurately detect the start of the frame sent by the transmitter. In this work, we consider the adoption of Barker Codes due to their good autocorrelation properties. In addition, we can append some '0' bits to the considered Barker Code to act as a waiting delay and reduce interference between the synchronisation

code and the information frame, thus resulting in a modified Barker Code. Figure 2 illustrates the frame structure where N_{BC} represents the length of the modified Barker Code and N_S denotes the number of information symbols.

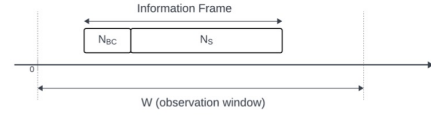


FIGURE 2. Frame structure.

B. CHANNEL MODEL

In MC, information molecules act as information carriers. However, the propagation of the molecules is induced by vibrations due to their thermal energy and collisions with other particles, making their movement purely random [17]. Therefore, the propagation of molecules in any medium can be described by the Brownian motion [7], [9], [17] which, in a three-dimensional space, can be modelled by

$$\begin{aligned} (x_{i+1}, y_{i+1}, z_{i+1}) &= (x_i + \mathcal{N}(0, 2D\Delta t)), \\ &[y_i + \mathcal{N}(0, 2D\Delta t)], \\ &[z_i + \mathcal{N}(0, 2D\Delta t)]. \end{aligned} \quad (1)$$

Hence, the position of an information molecule after a time interval (Δt) is given by its initial position (x_i, y_i, z_i), adding a spatial step $\mathcal{N}(0, 2D\Delta t)$ following a standard Gaussian distribution with mean 0 and variance $2D\Delta t$.

As shown in (1), the diffusion coefficient (D) has a direct impact on the movement of the information molecules. The mathematical model for this parameter can be described by the Stokes-Einstein relation as

$$D = \frac{k_B T}{\delta \pi \mu R} \quad [\text{m}^2/\text{s}] \quad (2)$$

where k_b is the Boltzmann constant ($k_b = 1.38 \times 10^{-23} \text{J/K}$), T is the temperature of the environment in Kelvin, μ is the viscosity of the fluid and R is the radius of the particle. Additionally, it is important to mention that δ is determined by the relation between the information molecules and the molecules in the fluid [9]. If the information molecules are bigger than the fluid particles, this parameter is equal to 6, if not, δ has a value of 4. For the investigation proposed in this paper, we consider a scenario where $\delta = 6$.

To fulfil the objectives proposed in this paper, we assume a transmission from a point transmitter to a fully-absorbing receiver [17]. The point transmitter considers the transmitter as a one-dimensional point where N_{molec} molecules are generated instantaneously, thus not taking into account either the geometry or the effects of the release of the molecules. Moreover, the model of a fully-absorbing receiver assumes that N_{rx} molecules are absorbed by the receiver's membrane during an observation window $[t_i, t_f]$, taking the geometry of the receiver into account. With this in mind, the probability

of an information molecule released at time $t = 0$ being absorbed by the molecular receiver at time t during the observation window can be obtained as [17]

$$F_{hit}(t_u - t_l) = \frac{a_{rx}}{d_0} \left[\operatorname{erfc} \left(\frac{d_0 - a_{rx}}{\sqrt{4Dt_u}} \right) - \operatorname{erfc} \left(\frac{d_0 - a_{rx}}{\sqrt{4Dt_l}} \right) \right] \quad (3)$$

where $\operatorname{erfc}()$ is the complementary error function, a_{rx} represents the radius of the considered receiver and d_0 is the distance between the centre of the transmitter and the centre of the receiver.

Assuming a time-invariant channel, we can define $\bar{h}[t, \tau]$ as the expected number of molecules absorbed at time t by the receiver, after a release of N_{molec} molecules at time τ .

$$\bar{h}[t, \tau] = N_{molec} F_{hit}(t, \tau). \quad (4)$$

Considering the diffusion of the molecules released by the transmitter and assuming the independency of the observations of the different molecules at the receiver, we adopt a Poisson distribution model which is commonly used in MC literature [11], [17], [18] as an accurate approximation to the binomial distribution that models the number of observed molecules. Therefore, to determine the concentration of the information molecules released at time τ and absorbed by the receiver at time interval t we use

$$h[t, \tau] \sim \text{Poisson}(\bar{h}[t, \tau]). \quad (5)$$

Furthermore, as already mentioned in section I, the molecular channel suffers from a high level ISI. Hence, taking this effect into account, it is possible to define the concentration of molecules observed at the k -th symbol as

$$y[k] = \sum_{l=0}^{L-1} h[l, k] x[k-l] + n[k] \quad (6)$$

where L is the channel memory length and $x[k]$ represents the k -th symbol modulated with binary CSK, thus $x[k] \in [A_0, A_1]$ where A_0 and A_1 represent the level for the bit '0' and '1', respectively. In addition, $n[k]$ represents the concentration of interfering molecules. These molecules are of the same type of the information carrying ones, even though they result from an independent process. As discussed in [11], they can be modelled using the same statistical distribution considered in (5), namely $n[k] \sim \text{Poisson}(\bar{n}[k])$.

At last, it is possible to define the concentration of information molecules observed by the receiver as

$$y[k] = \underbrace{\bar{h}[0, k] x[k]}_{\text{signal}} + \underbrace{n[k]}_{\text{environmental noise}} + \underbrace{v[k]}_{\text{diffusion noise}} + \underbrace{I[k]}_{\text{ISI}} \quad (7)$$

where the diffusion noise is modelled as a Poisson random variable whose mean has been subtracted. Hence, this variable is defined as $v[k] \sim \text{Poisson}_0(\bar{h}[0, k] x[k])$. Additionally, $I[k]$ represents the ISI effect and is given by $I[k] = \sum_{l=1}^{L-1} h[l, k] x[k-l]$.

III. SIGNAL DETECTION

The main goal of this work is to develop and study NN-based approaches for non-coherent detection and compare the performance against a direct non-coherent detection. The diagrams in figure 3 and 4 illustrate the main steps that are performed inside the receiver in order to obtain the final estimates of the information bits, using the two mentioned approaches.



FIGURE 3. Demodulation process for the direct non-coherent detection.



FIGURE 4. Demodulation process for the NN-based non-coherent detection.

A. DIRECT NON-COHERENT DETECTION

In this work, we consider the adoption of non-coherent detection, which means that the detection process is carried out without any CSI estimation. In the case of a conventional non data-driven approach as illustrated in figure 3, we apply a direct non-coherent detection to the received samples and, afterwards, we perform a hard bit decision to the soft estimates.

For computing soft symbol estimates in the direct non-coherent detector, we follow our previous work in [19]. First we define the number of received molecules in each position of the N_s bits that compose the information block i as $\mathbf{y}^i = (y^i[1], \dots, y^i[N_s])$. Additionally, considering a BCSK modulation scheme, the k -th symbol of information block i is represented by $x^i[k] \in [A_0, A_1]$, $k = 1, \dots, N_s$, where A_0 and A_1 denote the levels for bit '0' and '1', respectively, then, we define the probabilities $p_{1,k} = P(x^i[k] = A_1 | \mathbf{y}^i)$ and $p_{0,k} = P(x^i[k] = A_0 | \mathbf{y}^i)$ assuming an uniform distribution with bounds y_{min}^i and y_{max}^i , where $y_{min}^i = \min(\mathbf{y}^i)$ and $y_{max}^i = \max(\mathbf{y}^i)$. These probabilities can be computed as

$$p_{1,k} = \frac{y^i[k] - y_{min}^i}{y_{max}^i - y_{min}^i} \quad (8)$$

and

$$p_{0,k} = \frac{y_{max}^i - y^i[k]}{y_{max}^i - y_{min}^i}. \quad (9)$$

Using these probabilities it is possible to obtain the log-likelihood ratio (LLR) for each bit as

$$\lambda^i[k] = \log \left(\frac{p_{1,k}}{p_{0,k}} \right) \quad (10)$$

which allow us to write

$$p_{1,k} = \frac{1}{1 + e^{-\lambda^i[k]}}. \quad (11)$$

Bearing in mind that soft values are the conditional expected value of the received symbols, these can be calculated as

$$\tilde{x}^i[k] = E(x^i[k]|y^i) = (A_1 - A_0)p_{1,k} + A_0. \quad (12)$$

Finally, using (11), we can rewrite the expression for the computation of soft estimates as

$$\tilde{x}^i[k] = \frac{(A_1 + A_0)}{1 + e^{-\lambda^i[k]}} + A_0. \quad (13)$$

For OOK, we have $A_0 = 0$ and $A_1 = 1$ and (13) can be reduced to

$$\tilde{x}^i[k] = \frac{1}{2} \left(\tanh \left(\frac{\lambda^i[k]}{2} \right) + 1 \right). \quad (14)$$

Although we do not consider here, these soft symbol estimates can be used as input for a channel decoder when channel coding is employed. Since in this work we assume the transmission of uncoded information, we apply hard decision to the soft estimates coming from the direct non-coherent detector. Therefore, the k -th estimated bit of information block i , $\hat{x}^i[k]$, can be obtained as

$$\hat{x}^i[k] = \begin{cases} 0, & \tilde{x}^i[k] \leq \phi \\ 1, & \tilde{x}^i[k] > \phi, \end{cases} \quad (15)$$

where ϕ represents the threshold value and is given by $\phi = (A_0 + A_1)/2$. In the case of OOK, the threshold value becomes $\phi = 0.5$.

B. NEURAL NETWORK BASED DETECTION

As an alternative to the direct non-coherent detection, described above in section III-A, we propose a data-driven approach based on the implementation of NNs at the receiver. As it can be observed in figure 4, in this approach we apply a NN to the received samples in order to predict the information that was sent through the molecular channel. Similarly to the direct non-coherent detection, the adopted NN architectures output “soft” symbol estimates. Therefore, we apply hard bit decision to map these estimates into bits ‘0’ or ‘1’ using (15). Given that the molecular channel is very noisy and can be constantly changing, the received signal can vary considerably. Therefore, to address this challenge, in this work we adopted regression networks in order to obtain “soft” bit estimates, which are relevant for a channel decoder when the transmitted information is encoded. However, it is important to note that the architectures adopted can be easily adapted to classification based neural networks.

Finally, it is important to note that, given the constraints regarding MC, the proposed NNs were designed in order to achieve a good trade-off between the complexity of the NN and reliability, in terms of BER values achieved, for the molecular transmission. Two different architectures were considered: a 1-D CNN based on dilated causal convolutional layers and a GRU-RNN, as detailed next.

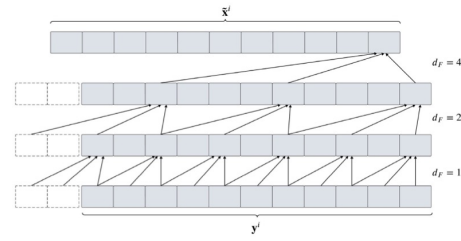


FIGURE 5. Architecture of a 1-D CNN based in dilated causal convolutional layers, adapted from [21].

1) 1-D CONVOLUTIONAL NEURAL NETWORK

The first NN-based approach proposed for accomplishing non-coherent detection of the information that passes through a molecular channel, corresponds to a low complexity 1-D CNN based on dilated causal convolutional layers architecture. The main feature of this CNN architecture is that it has the ability to memorise past inputs [20]. Therefore, bearing in mind that the molecular channel has memory, with this specific NN architecture, it is possible to take into account the temporal variations of the molecular channel.

The proposed NN is a variation of traditional CNNs. Specifically, the considered 1-D CNN is formed by dilated causal convolutional layers, which operate over the time steps of each sequence. In addition, one of the main features of these specific layers is that they are causal, meaning that each current output ($\tilde{x}^i[k]$) does not depend on future inputs [21]. The basic architecture of this NN is illustrated in figure 5. This NN is formed by convolutional layers with dilation, in order to increase the receptive field of each layer, without increasing the number of parameters. The dilation factor (d_F) determines the step size for sampling the input (y^i). Consequently, as the dilation factor increases, the distance between two consecutive filter taps also increases. The receptive field (R) is equivalent to the time steps of the input sequence used by the network for each estimate, which is calculated as

$$R = (f - 1)(2^J - 1) + 1 \quad (16)$$

for a stride of 1 and a dilation factor of 2^{j-1} at layer j , where f denotes the filter size and J is the number of convolutional layers in the NN.

In particular, we propose a deep NN comprising three one-dimension convolutional layers with a rectified linear unit (ReLU) activation function and a batch normalization layer between each of these layers. For the input layer, which inputs sequence data to the 1-D CNN, a data normalization is applied so that the input is rescaled to be in a range between 0 and 1. This network also includes a fully-connected layer as the output layer. Furthermore, each 1-D convolutional layer considers a stride of 1, a filter size of $f = 4$ and a causal method to determine the padding size, which is given by $p = (f - 1)d_F$, to ensure consistency in the size of the

frames along the network layers. Moreover, while the first 1-D convolutional layer has 2 filters, the other two have 4 filters. At last, to ensure a larger receptive field, the dilation factor increases exponentially in each convolutional layer, ranging from $d_F = 1$ to $d_F = 4$. In table 1, presented below, it is possible to observe the detailed architecture of this NN, as well as the parameters of each layer.

In this paper, all of the data used for training and validation of the NN was generated using Monte Carlo simulations. This dataset is independent from the data utilized for the find testing simulations. Therefore, we used a training and a validation dataset (N_{seq}) of 19200 sequences with a 99%/1% proportion using a length of $N_s = 20$ bits per frame. Given the large quantity of data, the dataset was divided into batches of 32 sequences to reduce overfitting and also to increase the performance and the accuracy of the network itself. Each sequence in the dataset is generated by first modulating a random sequence of 20 bits using binary CSK as described in section III-B, which represents the information that was transmitted. Afterwards, this information sequence passes through a time-invariant molecular channel modelled as (6), and onto which additive stationary noise is added. Therefore, each training pair that will feed the Neural Network will comprise this generated received sequence as well as the corresponding original information sequence in order to be used in the mean squared error loss function (17). The sequences used in the testing simulations are generated using a similar approach in order to be used in the loss function adopted for the NN.

Furthermore, we adopted the mean squared error loss function ($L_{MSE}(\theta)$), which is described as

$$L_{MSE}(\theta) = \frac{1}{N_{seq}} \sum_{i=1}^{N_{seq}} (f_{\theta}(\mathbf{y}^i) - \mathbf{x}^i)^2 \quad (17)$$

considering the NN as a function f_{θ} , where θ represents the learnable parameters. Additionally, \mathbf{y}^i and \mathbf{x}^i represent the i -th block of received molecules and information symbols, respectively. Moreover, the Adaptive Moment Estimation (Adam) method [22] is used as the optimisation algorithm, with an initial learning rate of 0.001. A maximum of 80 epochs were considered, where the training data is shuffled before each epoch to prevent overfitting. At last, the NN has a validation patience of 5, meaning that if after five attempts the loss function has not decreased its value, the training progress is stopped.

2) GATED RECURRENT UNIT BASED RECURRENT NEURAL NETWORK

As an alternative approach to the previous 1-D CNN, we propose a low complexity GRU-RNN to also perform non-coherent detection of the information sent through a molecular channel. Specifically, we adopt a three-layer GRU-RNN with a sequence input layer, two gated recurrent unit (GRU) layers and a fully-connected layer as the output layer.

GRU layers were proposed in [23] as a low complexity alternative to long short-term memory (LSTM) layers firstly introduced in 1997 by Hochreiter and Schmidhuber in [24]. Both these types of layers have the ability to learn long-term dependencies between data sequences. However, GRU layers have fewer parameters and a simpler architecture, making them more efficient. Figure 6 illustrates the structure of a GRU unit as adopted in this work. This unit relies in two different gate units that depend on the previous hidden state [23]: a reset gate (Γ_r) and an update gate (Γ_z). As the name suggests, the reset gate enables the unit to forget its previous state and the update gate determines how much the unit will be updated [25]. Both these two gates are computed with a sigmoid function (σ), which is applied to the current input (a_t) and to the previous value of the memory cell (b_{t-1}). Moreover, \tilde{b}_t is the candidate activation, which is updated at every timestep, and b_t is the output of the GRU unit at time t .

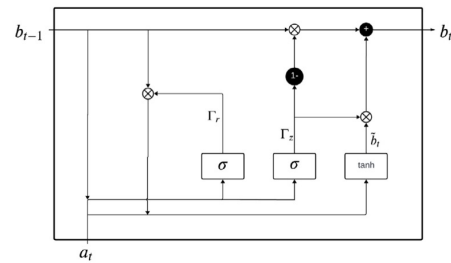


FIGURE 6. Structure of a GRU unit.

In the adopted GRU-RNN, the two GRU layers are implemented with 4 hidden units each. This was found to result in a good compromise between complexity and performance. The detailed architecture of this GRU-RNN is presented, in table 2.

Regarding the training parameters, this NN was trained with the same settings as the 1-D CNN described previously. Hence, a training and validation dataset was used, comprising 19200 sequences, each one with $N_s = 20$ bits per frame, divided into batches of 32 sequences to prevent overfitting. Adam was also used as the optimisation algorithm, with an initial learning rate of 0.001, and the mean squared error loss function, already described in (17). Finally, a validation patience of 5 and a maximum of 80 epochs was considered, where the training data is shuffled before each epoch.

It is important to highlight that the previously described NNs architectures were initially aimed at non-coherent molecular detection. However, as explained in the next section, they were also extended for scenarios where there is no prior synchronisation between the transmitter and the receiver. Hence, the proposed NN-based approaches are able to accomplish both synchronisation and non-coherent detection.

TABLE 1. 3 layer CNN architecture.

Layer	Type	Filter size	Filters	Dilation Factor	Activation	Learnable Parameters
1	Sequence input	–	–	–	–	–
2	1-D Convolutional	4	4	1	ReLu	20
3	Batch Normalization	–	–	–	–	8
4	1-D Convolutional	4	2	2	ReLu	34
5	Batch Normalization	–	–	–	–	4
6	1-D Convolutional	4	2	4	ReLu	18
7	Batch Normalization	–	–	–	–	4
8	Fully-connected	–	–	–	–	3

TABLE 2. GRU-RNN architecture.

Layer	Type	Hidden Units	Learnable Parameters
1	Sequence input	–	–
2	GRU	4	72
3	GRU	4	108
4	Fully-connected	–	5

C. FRAME SYNCHRONISATION

For the scenario where there is no prior synchronisation between the transmitter and the receiver, we propose three distinct methods for performing the synchronisation as well as the detection of the information sent from the transmitter to the receiver:

- **Method 1** - In this first method, a NN-based detection is implemented after a conventional synchronisation with the considered modified Barker Codes.
- **Method 2** - The second method relies on the implementation of a NN over the entire observation window of the receiver. Hence, in this case, we accomplish joint synchronisation and detection using a single NN.
- **Method 3** - With this method we propose the implementation of two different NNs, one for the synchronisation and another for the detection process.

In **method 1**, the NNs proposed in section III-B are only implemented for the detection process. Therefore, we apply conventional synchronisation, which relies on correlations between the received signal and the modified Barker Code along the whole observation window. The location of the maximum value for all the performed correlations is assumed to be the position of the synchronisation code in the observation window. Therefore, the position of the beginning of the information frame (\hat{k}_0) can be computed as

$$\hat{k}_0 = \operatorname{argmax}(\mathbf{c}^T \mathbf{y}[k : k + N_{BC} - 1]), \quad 0 \leq k \leq W - N_{BC} - N_s. \quad (18)$$

In this case, the bit sequence and the length of the modified Barker Code are represented by $\mathbf{c} = [c_0, \dots, c_{N_{BC}-1}]^T$ and N_{BC} , respectively. Moreover, N_s defines the total number of information symbols and W represents the size of the observation window. After obtaining the position of the synchronisation code, a NN is applied to the following 20 symbol positions in order to estimate the information that was received.

As for **method 2**, we follow an approach where a NN similar to the ones proposed in section III-B is applied to the entire observation window for accomplishing joint synchronisation and detection. As it can be observed in figure 7, we start by applying a NN to the whole observation window as is done in the case of the NN-based detection, thus obtaining soft bit estimates. Then, we perform a hard bit decision to the result in order to map the soft estimates onto bits '0' or '1', i.e., using (15). Afterwards, to find the beginning of the information frame, we apply a simple correlation between the estimated sequence and the Barker Code, similarly to (18). Finally, knowing the position of the synchronisation code in the observation window, we segment the frame by extracting the following N_s bits, which are considered to be the information that was sent by the transmitter.

Finally, for **method 3**, we propose the implementation of two different NNs also similar to the ones presented in section III-B: one for the synchronisation and another one for the detection process, as can be observed in figure 8. For this to be possible, we start by following an approach similar to method 2. However, after the correlation process to detect the beginning of the information frame, we segment the bit sequence \mathbf{y}^i . Then, we apply a NN-based detection to the resulting N_s samples in order to obtain soft bit estimates. Finally, using (15), we apply a hard decision to the soft estimates to map them into bits '0' or '1' to detect the information that was sent through the molecular channel.

IV. RESULTS

A. SIMULATION PARAMETERS

In this section, we present the results of the simulations conducted in this investigation, in order to evaluate the proposed NN-based approaches for MC.

Table 3 presents the main parameters considered for the simulations performed in this work. For this investigation, we consider the transmission of blocks of $N_s = 20$ bits using OOK as a modulation scheme with $A_0 = 0$, $A_1 = 1$ and $N_{molec} = 500$. Moreover, we consider a deterministic model of a point transmitter (tx), a spherical absorbing receiver (rx) and a Poisson distribution as a stochastic model for the channel. Furthermore, all simulations considered in this paper assume the transmission of uncoded unipolar non-return to zero (NRZ) signals where each sample corresponds to a symbol.

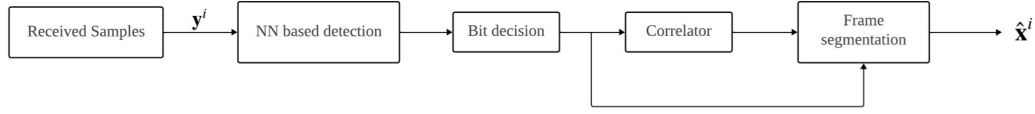


FIGURE 7. Demodulation process for method 2.

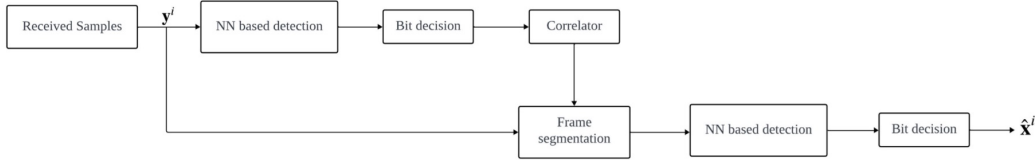


FIGURE 8. Demodulation process for method 3.

TABLE 3. Main parameters considered for the Monte Carlo simulations.

Parameters	Values
Molecules transmitted	500
Deterministic model	Point transmitter to Spherical absorbing receiver
Stochastic model	Poisson
Signal pulse type	Unipolar NRZ
Symbol duration (T_s)	$\alpha \cdot \frac{d_{tx-rx}^2}{6D}$ [s]
Modulation Scheme	OOK

Moreover, for the symbol duration (T_s), which has a significant impact on the transmission process, we used

$$T_s = \alpha \cdot \frac{d_{tx-rx}^2}{6D}. \quad (19)$$

It is important to note that, for all simulations presented in this paper, we have defined the scaling factor (α) as 1.

From (19), we can conclude that the diffusion coefficient (D) and the distance between the transmitter and the receiver (d_{tx-rx}) have a direct effect on the assumed symbol duration, which has a major influence on the ISI effect in the communication. Depending on the applications in which molecular communications are envisioned to be deployed, it is possible that the surrounding environment will be constantly changing. This implies that the transmitter and the receiver may move closer or further apart from each other, resulting in variations in the distance between these two devices. Furthermore, the diffusion coefficient, previously described in (2), influences the propagation speed of the information molecules through the molecular channel [17] and directly depends on the temperature and the viscosity of the environment. Thus, a variation in these parameters may change the value of the diffusion coefficient, which also has a significant impact on the transmission process. Since it is assumed that the transmitter and receiver have no knowledge of these variations, T_s is set with the expected distance and diffusion values.

In this investigation, we start always by evaluating the performance of the proposed NNs in a scenario where there are no variations in the distance and in the diffusion coefficient. Hence, we consider a distance between the transmitter and the receiver (d_{tx-rx}) of $10 \mu\text{m}$ and a value for the diffusion coefficient (D) of $79.4 \mu\text{m}^2/\text{s}$. Then, bearing in mind the influence that parameters such as the distance between the transmitter and the receiver and the diffusion coefficient have in the transmission process, we also present the results for a scenario considering variations of these parameters.

It is important to note that, following some experiments, it was decided to train both neural networks considering 100 dB in terms of signal to noise ratio (SNR), which is defined as N_{molec}/σ_n where σ_n^2 denotes the noise variance.

B. NEURAL NETWORK BASED DETECTION WITH PERFECT SYNCHRONISATION

In this section, we simulate a molecular transmission using the 1-D CNN and the GRU-RNN based detectors, which were previously described in section III-B, assuming perfect synchronisation between the transmitter and the receiver. For the analysis of the results, all simulations are compared with a direct non-coherent detection, using the approach described in section III-A.

The presented test results are obtained from simulations using a set of transmissions with 10000 frames each with $N_s = 20$ bits. Given that the quality of the communication directly depends on the channel conditions, the main objective is to evaluate the BER of the conventional molecular communication in comparison against a molecular communication where a NN-based approach is implemented for non-coherent detection.

As described in section III-B1 and III-B2, the training and validation datasets are composed by 19200 sequences, each with N_s bits per frame. In order to help verify the suitability of

the selected size for the training and validation datasets, the proposed 1-D CNN was trained with different dataset sizes, namely with 3840, 19200 and 38400 sequences. The results obtained for the different sets are illustrated in figure 9.

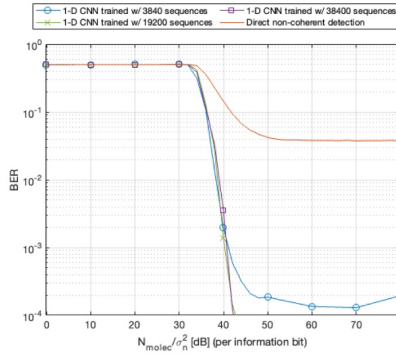


FIGURE 9. BER comparison between the NNs trained with different dataset sizes.

As expected, in figure 9 it is possible to observe that the NNs trained with 19200 and 38400 sequences exhibited better performance in comparison with the NN trained with only 3840 sequences. However, there is no apparent improvement in the performance between the NN trained with 19200 sequences and the one trained with 38400 sequences. Consequently, given the complexity constraints regarding MC, the training dataset with 19200 sequences revealed to be the most suitable option.

The decision to implement the specific 1-D CNN configuration, previously described in table 1, is justified by the superior complexity-performance trade-off exhibited by this specific NN architecture in comparison with other NNs with a greater number of layers. In order to help assess the advantage of the adopted three-layer NN architecture configuration, we compared it against other 1-D CNNs with different depths, namely five and seven one-dimensional convolutional layers. All NNs have a rectified linear unit (ReLU) activation function and a batch normalization layer between each one-dimensional convolutional layer. For the input layer, which inputs sequence data to each 1-D CNN, a data normalization is applied so that the input is rescaled to be in a range between 0 and 1. These networks also include a fully-connected layer as the output layer. In tables 4 and 5, it is possible to observe the detailed architecture of these additional 1-D CNNs, as well as the parameters of each layer. The comparison between the performance of these two NNs and of the NN from table 1 is illustrated in figure 10. It is important to note that due to the larger number of learnable parameters, a larger dataset was used for training these two deeper NNs.

From figure 10, it is possible to observe that there is no significant improvement in the performance of the NNs

comprising more convolutional layers in comparison with the three-layer NN. In addition, the reduced number of layers in the three-layer 1-D CNN results in a lower complexity NN when compared with the other considered 1-D CNN, which have a higher number of learnable parameters. Consequently, based on the presented results, we concluded that the three-layer 1-D CNN aligns effectively with the complexity constraints of MC due to its low-complexity, therefore being more suitable for the intended application.

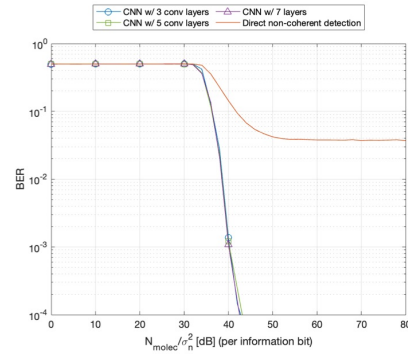


FIGURE 10. BER comparison between the NNs with different depths.

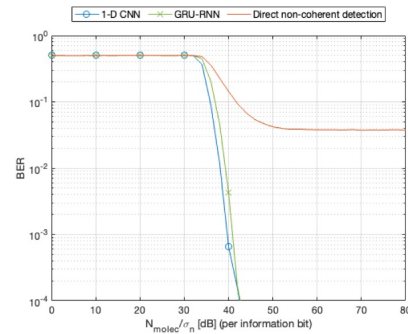


FIGURE 11. BER comparison between the NNs and the direct non-coherent detection.

Figure 11 illustrates a comparison between the BER of the conventional molecular communication and the NN-based non-coherent detection. As it can be seen in this figure, for SNR values above 42 dB, the proposed NNs can achieve BER values lower than 10^{-4} . This is a difference of three orders of magnitude when compared with the BER of the direct non-coherent detection, which has a BER floor value of 10^{-1} . In addition, it is possible to observe that, for both NNs, the value of the BER decreases for a SNR value higher than 30 dB, matching the behaviour of the direct non-coherent detection. At last, we can observe that both the proposed NN-based detectors have a similar performance.

TABLE 4. 5 layer CNN architecture.

Layer	Type	Filter size	Filters	Dilation Factor	Activation	Learnable Parameters
1	Sequence input	–	–	–	–	–
2	1-D Convolutional	2	8	1	ReLu	24
3	Batch Normalization	–	–	–	–	16
4	1-D Convolutional	2	4	1	ReLu	68
5	Batch Normalization	–	–	–	–	8
6	1-D Convolutional	4	4	1	ReLu	68
7	Batch Normalization	–	–	–	–	8
8	1-D Convolutional	4	2	2	ReLu	34
9	Batch Normalization	–	–	–	–	4
10	1-D Convolutional	4	2	4	ReLu	18
11	Batch Normalization	–	–	–	–	4
12	Fully-connected	–	–	–	–	3

TABLE 5. 7 layer CNN architecture.

Layer	Type	Filter size	Filters	Dilation Factor	Activation	Learnable Parameters
1	Sequence input	–	–	–	–	–
2	1-D Convolutional	2	16	1	ReLu	48
3	Batch Normalization	–	–	–	–	32
4	1-D Convolutional	2	8	1	ReLu	264
5	Batch Normalization	–	–	–	–	16
6	1-D Convolutional	3	8	1	ReLu	200
7	Batch Normalization	–	–	–	–	16
8	1-D Convolutional	3	4	1	ReLu	100
9	Batch Normalization	–	–	–	–	8
10	1-D Convolutional	4	4	1	ReLu	68
11	Batch Normalization	–	–	–	–	8
12	1-D Convolutional	4	2	2	ReLu	34
13	Batch Normalization	–	–	–	–	4
14	1-D Convolutional	4	2	4	ReLu	18
15	Batch Normalization	–	–	–	–	4
16	Fully-connected	–	–	–	–	3

Taking into account the previous results, in this testbed we also wanted to evaluate the impact of the variability of the channel conditions. Therefore, we simulated the performance of the proposed NNs, trained with a varying range of distances between the transmitter and the receiver and diffusion coefficient errors. For both the validation and the training process, we considered a range of distances between $5 \mu\text{m}$ and $15 \mu\text{m}$ and diffusion coefficient errors randomly changing between 5% and 15%. In addition, to cope with the expected variations in the molecular channel, which are assumed unknown at the receptor, the symbol duration parameter was modified in order to reduce the ISI effect. Hence, considering (19), d_{tx-rx} was set with a value of $15 \mu\text{m}$ whereas a maximum diffusion coefficient error of 15% was added to the standard value for the diffusion coefficient, resulting $D = 91.31 \mu\text{m}^2/\text{s}$.

In order to study the behaviour of the NNs in this scenario, in figure 12 we present the results for the original NNs trained both with and without the variations in the molecular channel. Comparing these results with the ones obtained in figure 11, we observe an increase in the BER for both NNs, regardless of the training method employed. This can be attributed to the more challenging nature of this scenario, as the considered variations in the distance between the transmitter and the receiver and in the diffusion coefficient, which are unknown at the receiver, lead to a significant deterioration of the

molecular transmission, thus increasing the BER. However, training both NNs under the effect of these variations improves the robustness, leading to a reduction in the overall BER of the molecular transmission for this scenario. We can observe a difference of approximately one order of magnitude when compared with a scenario where no NN is adopted or where a NN trained without considering variations in these parameters is used. Moreover, it is also noticeable that, independently of the training method, the BER for the GRU-RNN is slightly lower when compared with the BER achieved by the 1-D CNN.

C. NEURAL NETWORKS FOR THE DETECTION AND SYNCHRONISATION PROCESS

In this section we study the performance of the proposed NNs for a scenario where there is no previous synchronisation between the transmitter and the receiver. As already mentioned in section II-A, for this scenario we chose to employ a modified Barker Code for the synchronisation process. Hence, we consider a Barker Code of length 7, appending three additional '0' bits. Therefore, we consider the following synchronisation binary code: $\mathbf{c} = [1110010000]$. It is important to note that this specific synchronisation code was chosen after several simulations considering Barker Codes with different lengths. The considered synchronisation code

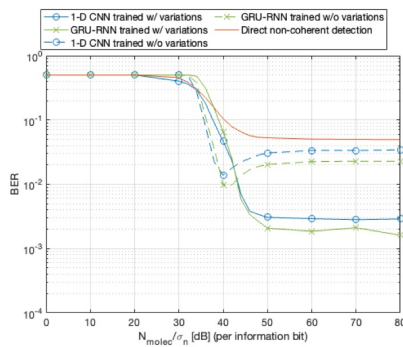


FIGURE 12. BER comparison between the NNs and the direct non-coherent detection, considering variations in the distance and in the diffusion coefficient.

is a trade-off between the complexity of the synchronisation process and the correct synchronism rate achieved.

Regarding the observation window, since it is assumed that initially the considered molecular receiver only detects an increase in the concentration of the information molecules, it will not be able to determine whether it detected the end or the beginning of the information frame. Hence, in this work, we consider that the receiver works with an observation window three times larger than the transmitted frame. Therefore, for a frame of $N_s = 20$ bits and a modified Barker Code with a total of $N_{BC} = 10$ bits, the receiver has an observation window of $W = 90$ bits, plus the maximum channel memory length which is considered to be of $L = 7$ symbols.

Finally, it is important to mention that all the simulations presented in this section are compared with a direct non-coherent detection, where no NN is applied.

To evaluate the performance of the NNs for each of the proposed methods, we consider the same parameters and values described in section IV-A. Moreover, we present the results of the BER and the synchronisation rate as a function of N_{molec}/σ_n , in order to observe the evolution of the accuracy of each method. Additionally, it must be noted that the BER results only consider the cases where the synchronism was correct.

From the analysis of figure 13.a) we can conclude that, for each method, both of the proposed NNs have a similar behaviour. Finally, it is important to mention that, since the detection process is the same for method 1 and method 3, the results for these methods are illustrated in the same plot line.

As it can be seen in figure 13.b), since both method 1 and the direct non-coherent detection apply a conventional correlation for the synchronisation process, the results for these two scenarios are illustrated in the same plot line. Moreover, we can observe that, in this case, there is an increase in the rate of correct synchronisms for SNR

values between 10 dB and 40 dB, achieving a successful synchronisation rate above 90% for values over 40 dB. Although method 1 shows better synchronisation rates for SNRs below 35 dB, it corresponds to a scenario in which the BER is very high, approaching 50%, therefore making it less relevant. In contrast, for method 2 we can observe synchronisation rates of 100% for values of 40 dB and above for both NNs. However, it is important to note that, for this case, the synchronisation rate only starts to increase at SNRs around 35 dB but it quickly reaches its maximum value. Finally, for method 3, we can observe that the synchronisation rate is identical for both of the proposed NNs. In addition, this method has a similar performance to method 2. However, since this method relies in the implementation of two NNs, the synchronisation and detection process incurs in a higher complexity when compared with method 2.

Bearing in mind the previous results, in the following testbed we evaluate the performance of the proposed NNs for each of the previously mentioned methods of synchronism, considering a scenario with variations in the distance between the transmitter and the receiver as well as the diffusion coefficient. For this to be possible, we consider a range of distances between $5 \mu\text{m}$ and $15 \mu\text{m}$ and diffusion coefficient errors randomly varying between 5% and 15% for both the training and the validation process.

As it can be seen in figure 14.a), for each of the considered methods, the NNs that were trained considering variations in the distance and in the diffusion coefficient have a better performance, achieving lower BER values when compared with the other scenarios. In addition, we observe that, for all methods, the proposed GRU-RNN has a lower BER floor value when compared with the 1-D CNN. Moreover, it is noticeable that, for method 1 and 3, the BER value of the 1-D CNN trained with variations decreases for a SNR value higher than 20 dB, surpassing the behaviour of the direct non-coherent detection.

Regarding the synchronisation rate, illustrated in figure 14.b), we can observe a significant reduction in the synchronisation rate for the direct non-coherent detection (and for method 1 since this also implements a conventional synchronisation). Unlike the 90% synchronisation rate achieved previously in figure 13.b), in this case it is only possible to achieve a maximum synchronisation rate around 84%. As for method 2, unlike what was observed in figure 13.b), for both NNs trained considering variations in the distance and in the diffusion coefficient, it is only possible to achieve a synchronisation rate of 100% for N_{molec}/σ_n values of approximately 45 dB and above. For method 3, it is possible to observe that the synchronisation rate for the 1-D CNN trained with variations starts to increase from SNR values of 20 dB and above. At last, it is noticeable that, for the GRU-RNN, it is possible to achieve a synchronisation rate of 100% for N_{molec}/σ_n values of approximately 45 dB and above. However, for the 1-D CNN, it is only possible to achieve a maximum synchronisation rate of approximately 96%. In contrast, the same does not occur when the proposed

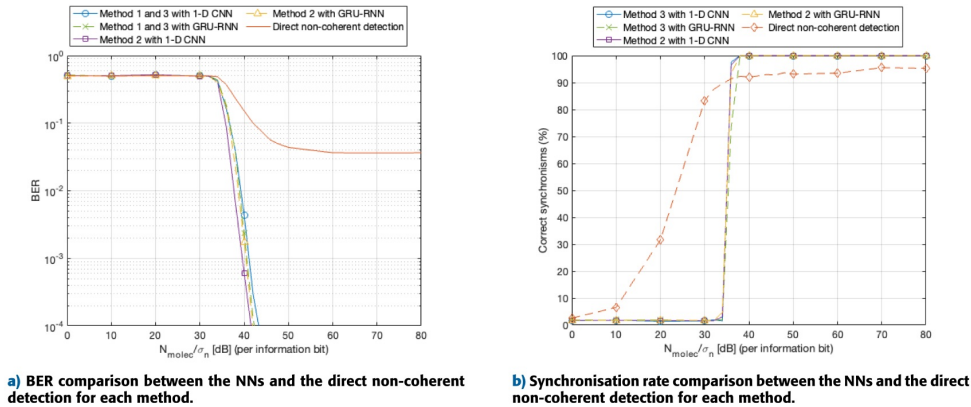


FIGURE 13. NNs applied to each synchronisation and detection method.

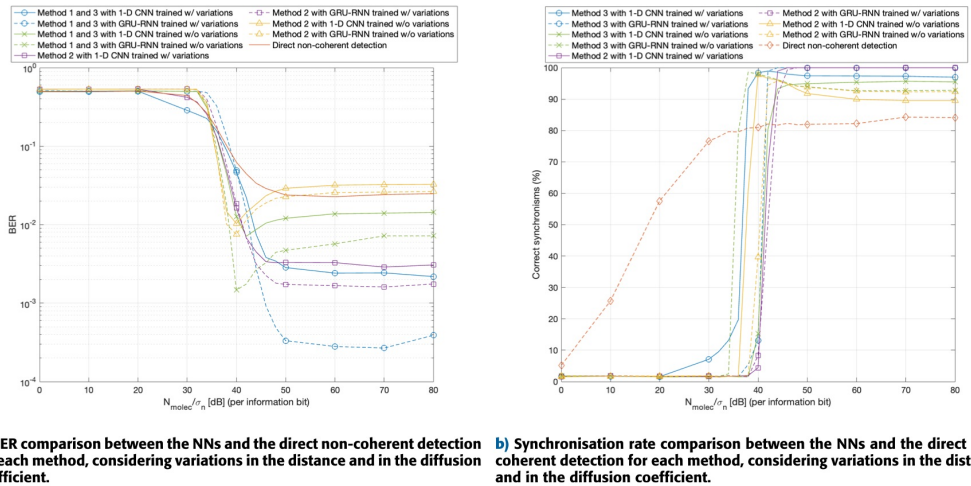
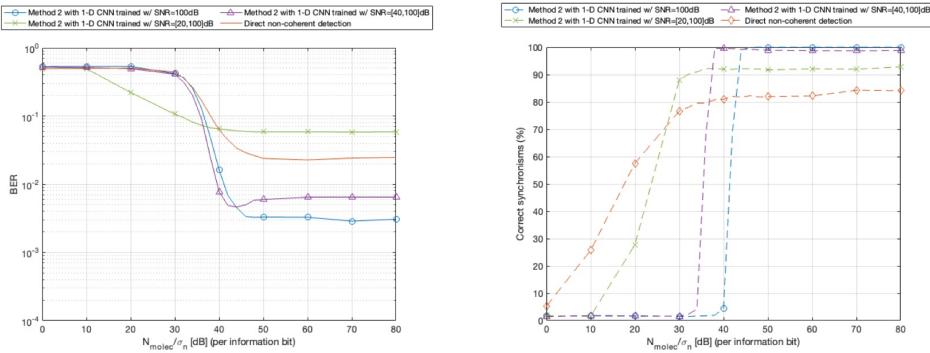


FIGURE 14. NNs applied to each synchronisation and detection method, considering variations in the distance and in the diffusion coefficient.

NNs are trained without considering variations in the distance and in the diffusion coefficient.

To provide further analysis regarding the behaviour of the proposed NNs under noisy conditions, in the following results we evaluate the impact of the type of data used for training, namely how the level of noise present on the training sequences influences the performance of the proposed NN based synchronisation and detection schemes. Therefore, figure 15 presents the results of the proposed 1-D CNN trained with datasets covering different ranges of SNR values. For this evaluation, and considering the previous results we selected method 2 since, while it exhibits slightly worse performance in terms of BER, it presents a higher correct

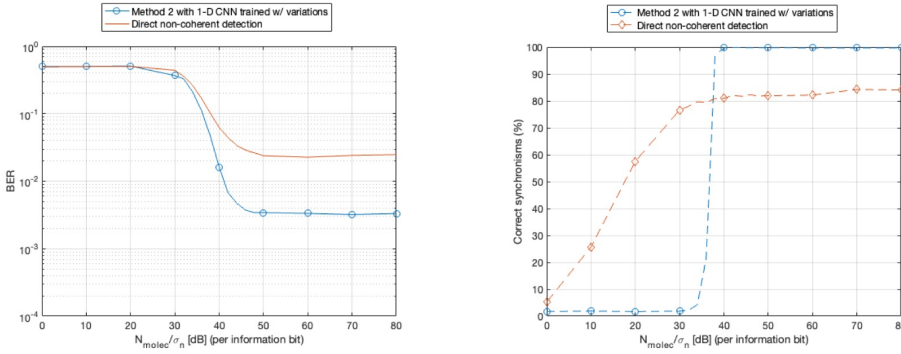
synchronisation rate when compared to method 3. Moreover, method 2 relies on a single NN for joint synchronisation and detection, making it less computationally complex than method 3, which relies on two separate NNs. In figure 15.a), we can observe that the NN trained with a SNR value of 100 dB exhibits better performance, achieving lower BER values than the other considered NNs. In comparison, the NNs trained with a large interval of SNR values achieve lower BER values for lower N_{molec}/σ_n values. However, for higher N_{molec}/σ_n values, the BER floor value for these NNs becomes higher in comparison with the NN trained with a single SNR value of 100 dB. Moreover, as it can be observed in figure 15.b), the NN trained with a SNR value



a) BER comparison between the NNs trained with different SNR values and the direct non-coherent detection, considering variations in the distance and in the diffusion coefficient.

b) Synchronisation rate comparison between the NNs trained with different SNR values and the direct non-coherent detection, considering variations in the distance and in the diffusion coefficient.

FIGURE 15. 1-D CNN trained with different SNR values applied to method 2, considering variations in the distance and in the diffusion coefficient.



a) BER comparison between the NN and the direct non-coherent detection, considering variations in the distance and in the diffusion coefficient in a time-variant channel.

b) Synchronisation rate comparison between the NN and the direct non-coherent detection, considering variations in the distance and in the diffusion coefficient in a time-variant channel.

FIGURE 16. 1-D CNN applied to method 2, considering variations in the distance and in the diffusion coefficient in a time-variant channel.

of 100 dB achieves a correct synchronisation rate of 100% for N_{molec}/σ_n values of 45 dB and above. In comparison, the NNs trained with an interval of SNR values achieve higher synchronisation rates for lower N_{molec}/σ_n values. However, for higher N_{molec}/σ_n values, these NNs achieve lower synchronisation rates than that achieved by the NN trained with a SNR value of 100 dB. These results seem to suggest that while training the NN using some sequences corrupted by higher levels of noise may provide some additional robustness when operating in worse conditions, it can severely limit the performance that can be achieved in more favourable scenarios.

All the results presented previously consider a time-invariant molecular channel. However, to assess the

robustness of the proposed approach, we extend this investigation for a scenario considering a time-variant molecular channel with unknown variations in the distance between the transmitter and the receiver and in the diffusion coefficient. In this case, for the time-variant channel it is assumed that the expected number of molecules absorbed at each time t by the receiver, as given by (3) and (4), will change for each release time τ , due to random variations on the diffusion coefficient. This provides a further analysis of the impact of stochastic variations in the channel on the performance of the proposed NN-based non-coherent detection and synchronisation schemes. As already mentioned, given that method 2 is less complex than method 3, we simulate the results for the considered

1-D CNN applied to method 2, properly trained considering a time-variant molecular channel with unknown variations in the distance and in the diffusion coefficient. As can be seen in figure 16.a), the considered NN still exhibits lower BER values when compared with the direct non-coherent detection. Moreover, as illustrated in figure 16.b), we can observe that the proposed 1-D CNN applied to method 2 achieves a synchronisation rate of 100% for N_{molec}/σ_n values of approximately 40 dB and above, therefore providing more robustness than the conventional direct approach.

V. CONCLUSION

Molecular Communication has the potential to be at the heart of IoBNT due to its revolutionary capabilities that transcend traditional communication systems. However, the unpredictable nature of the molecular channel induces environment noise and causes high ISI interference, making these two of the main challenges to overcome regarding this type of communication. To help address these problems, in this paper we propose a low complexity 1-D CNN comprising dilated causal convolutional layers and a GRU-RNN based approach, both aimed at achieving non-coherent detection and synchronisation in MC receivers, in order to increase the robustness of the molecular transmission.

Initially, we described these data-aided NNs-based approaches for accomplishing detection, assuming that the transmitter and the receiver were previously synchronised. For this scenario, it was observed that both of the proposed NNs perform significantly better when compared with a direct non-coherent detection, with the GRU-RNN having lower complexity and a slightly better performance when compared with the 1-D CNN.

Subsequently, we have extended the two NN architectures for scenarios where there is no prior synchronisation between the transmitter and the receiver, proposing two different synchronisation methods. In this part of our study, we have concluded that the implementation of the NNs for the synchronisation process increases the correct synchronisation rate, thus adding greater robustness to the molecular transmission. Moreover, comparing the use of a single NN for joint synchronisation and detection against the use of two separate NNs for synchronisation and detection, it was observed that the later achieves a better performance in terms of BER. However, this is not the case when considering the synchronisation rate, which is very similar for both methods.

Finally, in this work, we also investigated the behaviour of the proposed NNs for scenarios where there are unknown variations in the distance and in the diffusion coefficient. Given this more challenging setting, it was observed that the proposed NN-based non-coherent detection and synchronisation schemes can provide more robustness than a conventional non-data aided approach.

REFERENCES

- [1] W. Guo, M. Abbaszadeh, L. Lin, J. Charmet, P. Thomas, Z. Wei, B. Li, and C. Zhao, "Molecular physical layer for 6G in wave-denied environments," *IEEE Commun. Mag.*, vol. 59, no. 5, pp. 33–39, May 2021.
- [2] I. F. Akyildiz, M. Pierobon, S. Balasubramaniam, and Y. Koucheryavy, "The Internet of Bio-Nano Things," *IEEE Commun. Mag.*, vol. 53, no. 3, pp. 32–40, Mar. 2015.
- [3] N. Farsad, H. B. Yilmaz, A. Eckford, C.-B. Chae, and W. Guo, "A comprehensive survey of recent advancements in molecular communication," *IEEE Commun. Surveys Tuts.*, vol. 18, no. 3, pp. 1887–1919, 3rd Quart., 2016.
- [4] Y. Huang, F. Ji, Z. Wei, M. Wen, and W. Guo, "Signal detection for molecular communication: Model-based vs. data-driven methods," *IEEE Commun. Mag.*, vol. 59, no. 5, pp. 47–53, May 2021.
- [5] J. M. Jornt and A. Sangwan, "Nanonetworking in the terahertz band and beyond," *IEEE Nanotechnol. Mag.*, vol. 17, no. 3, pp. 21–31, Apr. 2023.
- [6] T. Nakano, M. J. Moore, F. Wei, A. V. Vasilakos, and J. Shuai, "Molecular communication and networking: Opportunities and challenges," *IEEE Trans. Nanobiosci.*, vol. 11, no. 2, pp. 135–148, Jun. 2012.
- [7] L. Chouhan and M.-S. Alouini, "Interfacing of molecular communication system with various communication systems over Internet of Every Nano Things," *IEEE Internet Things J.*, vol. 10, no. 16, pp. 14552–14568, Aug. 2023.
- [8] H. Zhai, Q. Liu, A. V. Vasilakos, and K. Yang, "Anti-ISI demodulation scheme and its experiment-based evaluation for diffusion-based molecular communication," *IEEE Trans. Nanobiosci.*, vol. 17, no. 2, pp. 126–133, Apr. 2018.
- [9] M. S. Kuran, H. B. Yilmaz, I. Demirkol, N. Farsad, and A. Goldsmith, "A survey on modulation techniques in molecular communication via diffusion," *IEEE Commun. Surveys Tuts.*, vol. 23, no. 1, pp. 7–28, 1st Quart., 2021.
- [10] S. Lotter, L. Brand, V. Jamali, M. Schäfer, H. M. Loos, H. Unterweger, S. Greiner, J. Kirchner, C. Alexiou, D. Drummer, G. Fischer, A. Buettner, and R. Schober, "Experimental research in synthetic molecular communications—Part I," *IEEE Nanotechnol. Mag.*, no. 3, 2023.
- [11] V. Jamali, N. Farsad, R. Schober, and A. Goldsmith, "Non-coherent detection for diffusive molecular communication systems," *IEEE Trans. Commun.*, vol. 66, no. 6, pp. 2515–2531, Jun. 2018.
- [12] M. Bartunik, J. Kirchner, and O. Keszocze, "Artificial intelligence for molecular communication," *Inf. Technol.*, vol. 65, nos. 4–5, pp. 155–163, Aug. 2023, doi: 10.1515/itit-2023-0029.
- [13] N. Farsad and A. Goldsmith, "Neural network detection of data sequences in communication systems," *IEEE Trans. Signal Process.*, vol. 66, no. 21, pp. 5663–5678, Nov. 2018.
- [14] M. Bartunik, O. Keszocze, B. Schiller, and J. Kirchner, "Using deep learning to demodulate transmissions in molecular communication," in *Proc. IEEE 16th Int. Symp. Med. Inf. Commun. Technol. (ISMICT)*, May 2022, pp. 1–6.
- [15] V. Sze, Y.-H. Chen, T.-J. Yang, and J. S. Emer, "Efficient processing of deep neural networks: A tutorial and survey," *Proc. IEEE*, vol. 105, no. 12, pp. 2295–2329, Dec. 2017.
- [16] Y. Lecun, Y. Bengio, and G. Hinton, "Deep learning," *Nature*, vol. 521, no. 7553, pp. 436–444.
- [17] V. Jamali, A. Ahmadzadeh, W. Wicke, A. Noel, and R. Schober, "Channel modeling for diffusive molecular communication—A tutorial review," *Proc. IEEE*, vol. 107, no. 7, pp. 1256–1301, Jul. 2019.
- [18] M. Kuscü, E. Dinc, B. A. Bilgin, H. Ramezani, and O. B. Akan, "Transmitter and receiver architectures for molecular communications: A survey on physical design with modulation, coding, and detection techniques," *Proc. IEEE*, vol. 107, no. 7, pp. 1302–1341, Jul. 2019.
- [19] S. Figueiredo, N. Souto, and F. Cercas, "Low-complexity channel codes for reliable molecular communication via diffusion," *Sensors*, vol. 22, no. 1, pp. 41–55, Dec. 2021. [Online]. Available: <https://search.ebscohost.com/login.aspx?direct=true&db=edspsc&AN=000741422400001&site=eds-live>
- [20] C. Lea, M. D. Flynn, R. Vidal, A. Reiter, and G. D. Hager, "Temporal convolutional networks for action segmentation and detection," in *Proc. IEEE Conf. Comput. Vis. Pattern Recognit. (CVPR)*, Jul. 2017, pp. 1003–1012.
- [21] S. Bai, J. Zico Kolter, and V. Koltun, "An empirical evaluation of generic convolutional and recurrent networks for sequence modeling," 2018, *arXiv:1803.01271*.
- [22] D. P. Kingma and J. Ba, "Adam: A method for stochastic optimization," 2014, *arXiv:1412.6980*.
- [23] K. Cho, B. van Merriënboer, D. Bahdanau, and Y. Bengio, "On the properties of neural machine translation: Encoder–decoder approaches," 2014, *arXiv:1409.1259*.

- [24] S. Hochreiter and J. Schmidhuber, "Long short-term memory," *Neural Comput.*, vol. 9, no. 8, pp. 1735–1780, Nov. 1997. [Online]. Available: <https://search.ebscohost.com/login.aspx?direct=true&db=cmedm&AN=9377276&site=eds-live>
- [25] J. Chung, C. Gulcehre, K. Cho, and Y. Bengio, "Empirical evaluation of gated recurrent neural networks on sequence modeling," 2014, *arXiv:1412.3555*.



DUARTE CASALEIRO received the degree in telecommunications and computer engineering from the Iscte–Instituto Universitário de Lisboa, Lisbon, Portugal, in 2022, where he is currently pursuing the M.S. degree in telecommunications and computer engineering, with specialization in the Internet of Things. His research interests include molecular communication and machine learning for wireless communications.



NUNO M. B. SOUTO (Senior Member, IEEE) received the Graduate, Ph.D., and Habilitation degrees in aerospace engineering from the Avionics Branch, Instituto Superior Técnico, Lisbon, Portugal, in 2000, 2006, and 2021, respectively. From November 2000 to January 2002, he was a Researcher in the field of automatic speech recognition with the Instituto de Engenharia e Sistemas de Computadores, Lisbon. He joined the Iscte–University Institute of Lisbon, as an Assistant Professor, in 2006. He has been a Researcher with the Instituto de Telecomunicações (IT), Portugal, since 2002, and has been involved in several international research projects and many national projects. His research interests include wireless networks, signal processing for communications, multicarrier communications, frequency domain equalization, channel coding, modulation, channel estimation, synchronization, MIMO schemes, wireless sensor networks, unmanned aerial vehicles, mmWave/terahertz communications, machine learning for wireless communications, and molecular communications. He is a member of the IEEE Communications Society, the IEEE Signal Processing Society, and the IEEE Instrumentation and Measurement Society.



JOÃO C. SILVA received the B.S. degree in aerospace engineering from the Instituto Superior Técnico (IST), Lisbon Technical University, in 2000, and the M.B.A. degree from ISEG, in 2015. He finished his Ph.D. thesis at IST, in 2006, focusing on spread spectrum techniques, multiuser detection schemes, and MIMO systems. From 2000 to 2002, he was a Business Consultant with McKinsey & Company. Since 2006, he has been working on computer networks as an Assistant Professor with ISCTE-IUL.

...